Universidad de Málaga

Escuela Técnica Superior de Ingeniería de Telecomunicación

TESIS DOCTORAL

Study of MIMO techniques for Power Line Communications

Autor:

JULIO ALBERTO CORCHADO LÓPEZ

Doctorado en Ingeniería de Telecomunicación

Ph.D. in Electronics and Telecommunications

Directores:

LUIS DÍEZ DEL RÍO

JOSÉ ANTONIO CORTÉS ARRABAL

AÑO 2023

AUTOR: Julio Alberto Corchado López
https://orcid.org/0000-0001-6244-5265

EDITA: Publicaciones y Divulgación Científica. Universidad de Málaga

DECLARACIÓN DE AUTORÍA Y ORIGINALIDAD DE LA TESIS PRESENTADA PARA OBTENER EL TÍTULO DE DOCTOR

D./Dña JULIO ALBERTO CORCHADO LÓPEZ
Estudiante del programa de doctorado INGENIERÍA DE TELECOMUNICACIÓN de la Universidad de Málaga, autor/a de la tesis, presentada para la obtención del título de doctor por la Universidad de Málaga, titulada: STUDY OF MIMO TECHNIQUES FOR POWER LINE COMMUNICATIONS.
Realizada bajo la tutorización de LUIS DÍEZ DEL RÍO y dirección de JOSÉ ANTONIO CORTÉS ARRABAL Y LUIS DÍEZ DEL RÍO (si tuviera varios directores deberá hacer constar el nombre de todos)

DECLARO QUE:

La tesis presentada es una obra original que no infringe los derechos de propiedad intelectual ni los derechos de propiedad industrial u otros, conforme al ordenamiento jurídico vigente (Real Decreto Legislativo 1/1996, de 12 de abril, por el que se aprueba el texto refundido de la Ley de Propiedad Intelectual, regularizando, aclarando y armonizando las disposiciones legales vigentes sobre la materia), modificado por la Ley 2/2019, de 1 de marzo.

Igualmente asumo, ante a la Universidad de Málaga y ante cualquier otra instancia, la responsabilidad que pudiera derivarse en caso de plagio de contenidos en la tesis presentada, conforme al ordenamiento jurídico vigente.

En Málaga, a 23 de DICIEMBRE de 2023

Fdo.: JULIO ALBERTO CORCHADO LÓPEZ Doctorando/a	Fdo.: LUIS DÍEZ DEL RÍO Tutor/a
Fdo.: JOSÉ ANTONIO CORTÉS ARRABAL Y LUIS DÍEZ DEL RÍO Director/es de tesis	

Edificio Pabellón de Gobierno. Campus El Ejido. 29071
Tel.: 952 13 10 28 / 952 13 14 61 / 952 13 71 10
E-mail: doctorado@uma.es

AUTORIZACIÓN PARA LA LECTURA DE LA TESIS POR COMPENDIO DE PUBLICACIONES

D. Luis Díez del Río y D. José Antonio Cortés Arrabal, profesores doctores del departamento de Ingeniería de Comunicaciones de la Universidad de Málaga

CERTIFICAN

Que D. Julio Alberto Corchado López, Ingeniero de Telecomunicación, ha realizado en el departamento de Ingeniería de Comunicaciones de la Universidad de Málaga, bajo su dirección el trabajo de investigación correspondiente a su TESIS DOCTORAL titulada:

"Estudio de técnicas MIMO en entornos PLC"/"Study of MIMO techniques for Power Line Communications"

En dicho trabajo se han realizado contribuciones en el ámbito de la caracterización de la correlación espacial de los canales MIMO (*multiple-input multiple-output*) PLC (*power line communications*), tanto en lo referente a la respuesta del canal como el ruido. Además, se ha propuesto un modelo para la respuesta de los canales MIMO que refleja la citada correlación de manera más realista que los modelos existentes en la literatura. Estos resultados han dado lugar a las siguientes publicaciones:

- Julio A. Corchado, José A. Cortés, Francisco J. Cañete, and Luis Díez, "An MTL-Based Channel Model for Indoor Broadband MIMO Power Line Communications", IEEE Journal on Selected Areas in Communications, Vol. 34, No. 7, pp. 2045-2055, July 2016. DOI: 10.1109/JSAC.2016.2566178
- Julio A. Corchado, José A. Cortés, Francisco J. Cañete, Antonio Arregui, and Luis Díez, "Analysis of the Spatial Correlation of Indoor MIMO PLC Channels", IEEE Communications Letters, Vol. 21, No. 1, pp. 40-43, January 2017. DOI: 10.1109/LCOMM.2016.2616341
- José A. Cortés, Julio A. Corchado, Francisco J. Cañete and Luis Díez, "Analysis and Exploitation of the Noise Correlation in MIMO Power Line Communications in the FM Band", IEEE Comm. Letters, Vol. 22, No. 3, pp. 566-569, March 2018. DOI: 10.1109/LCOMM.2017.2787714

Respecto a estas publicaciones, la tesis por compendio realiza una introducción más prolija de las comunicaciones por redes eléctricas y sus ámbitos de aplicación, describe las características de los canales PLC de manera más amplia y detallada y actualiza el análisis del estado de la cuestión.

Por todo ello, los directores consideran que esta tesis es apta para su presentación al Tribunal que ha de juzgarla y AUTORIZAN la presentación de la tesis por COMPENDIO DE PUBLICACIONES en la Universidad de Málaga. Igualmente, certifican que las publicaciones que avalan la tesis no han sido empleadas en trabajos anteriores a la misma.

En Málaga, a 23 de diciembre de 2023

Fdo.: Luis Díez del Rio

Fdo.: José Antonio Cortés Arrabal

UNIVERSIDAD DE MÁLAGA

ESCUELA TÉCNICA SUPERIOR DE INGENIERÍA DE TELECOMUNICACIÓN

Reunido el tribunal examinador en el día de la fecha, constituido por:

Presidente: Dr. D. _____

Secretario: Dr. D. _____

Vocal: Dr. D. _____

para juzgar la Tesis Doctoral titulada "*Study of MIMO techniques for Power Line Communications*", realizada por D. Julio Alberto Corchado López y dirigida por los Dres. D. Luis Díez del Río y D. José Antonio Cortés Arrabal,

acordó por _____ otorgar la calificación de

_____

y, para que conste, se extiende firmada por los componentes del tribunal la presente diligencia.

Málaga, a _____ de _____ del _____

El presidente: El secretario: El vocal:

Fdo.: _____ Fdo.: _____ Fdo.: _____

"Perseverance is not a long race; it is many short races one after the other."

Walter Elliot

Acknowledgements

I would like to express my sincere gratitude to the following individuals who have played a significant role in my academic journey and the completion of this dissertation:

First of all, my deepest appreciation goes to my thesis supervisors, José Antonio and Luis. Their expertise, guidance, and unending patience have been instrumental in shaping this research. Without their mentorship and support, I would have succumbed to the challenges of this endeavor long ago. Their dedication to my academic growth has been invaluable.

I am immensely grateful to my parents, Julio and Eli, for their unwavering support, encouragement, and belief in my abilities. Your love and guidance have been my greatest source of strength throughout this journey. I also want to thank my younger brother, Alex, who has been a constant source of motivation.

I extend my gratitude to my colleagues at the university, especially Adrián, who has been a source of inspiration and collaboration throughout this academic journey. Your camaraderie, shared insights, and collaborative spirit have enriched my experience and contributed to the success of this research. I am honored to have been part of such a supportive academic community.

To all those whose names may not be mentioned but whose contributions, however small or significant, have played a part in the completion of this dissertation, I extend my heartfelt thanks.

This work stands as a testament to the collaborative efforts of many, and I am profoundly grateful for the support and encouragement I have received along the way.

Declaration of Authorship

I, Julio Alberto Corchado López, declare that this thesis titled, "Study of MIMO techniques for Power Line Communications" and the work presented in it are my own. I confirm that:

- This work was done wholly while in candidature for a research Ph. D. degree at this University.
- This work has not been submitted for any other degree or award in any other University or Educational Institution.
- Where I have consulted the published work of others, this is always clearly attributed.
- Where I have quoted from the work of others, the source is always given. With the exception of such quotations, this thesis is entirely my own work.
- I have acknowledged all main sources of help.

Julio Alberto Corchado López
Department of Communication Engineering
University of Málaga
March 17, 2024

Abstract

Power line communication (PLC) consists in the exchange of information over electrical cables. PLC takes advantage of the ubiquity of already deployed power delivery networks and provides access to telecommunication services without any further infrastructure installation. Furthermore, the propagation of PLC signals is insensitive to wall/floor thickness, therefore they can propagate in multi-storey premises much better than wireless.

PLC applications are generally categorized as either outdoor or indoor. Outdoor applications usually take place over the distribution power network and the signal travel distance may be of up to a few kilometers. A well-known application of outdoor PLC systems is smart metering. On the other hand, indoor applications are usually focused on, but not restricted to, providing high data rate connectivity inside buildings. In both cases, PLC can complement wireless communication systems to improve coverage. Moreover, PLC systems can also be classified into narrowband (NB) and broadband (BB) systems. The work presented herein focuses on the latter.

Traditionally, PLC systems used only two conductors, thus resulting in a single-input single-output (SISO) system. However, most indoor power lines are composed of three conductors, and this third conductor can be exploited to enable a multiple-input multiple-output (MIMO) system over this channel. Exploitation of MIMO capabilities enhance the achievable performance over a given medium. MIMO features have been extensively studied for wireless environments but MIMO in wired scenarios show some distinct aspects with respect to their wireless counterparts. In particular, the channels that make up the MIMO PLC link show a closer relation (higher spatial correlation) than in their wireless counterpart. This higher spatial correlation can be observed in both, the channel response and noise of the MIMO PLC channel. Regarding the channel response, a higher spatial correlation

entails a lower MIMO performance gain, whereas highly correlated noise can be exploited to achieve higher MIMO performance gains. However, nowadays the channel spatial correlation dependence with frequency (both in the channel response and noise) is unknown, as it is unknown the relationship of the channel response spatial correlation to the physical features of the network, such as the type of wiring, the type of deployment, etc. Furthermore, existing MIMO channel response models do not reflect an accurate representation of the spatial correlation observed in measurements. MIMO PLC models and transmission strategies need to take into account these particularities to take full advantage of MIMO capabilities.

The first contribution of this work is a multiconductor transmission line (MTL)-based MIMO PLC model which captures spatial correlation in a way that other MTL-based models cannot. Three modifications on the channel model are proposed to achieve this: modified loads, branches and cabling. The proposed model leads to MIMO channels similar to the measured ones, both in terms of the characteristics of their individual SISO channels and of the correlation between them.

The second contribution shows, by means of measurements, that spatial correlation in PLC channel responses does not display a significant dependence with respect to frequency, just like in the typical wireless MIMO scenario, and that there exist alternative injection modes to the usual differential one, like the pseudo-differential injection, which yield lower spatially correlated MIMO channels.

Lastly, the third contribution provides a characterization of the noise correlation in MIMO PLC in the 2-108 MHz band, showing that noise in the frequency modulation (FM) band displays very high spatial correlation. It has been proven that the exploitation of the aforesaid correlation, by means of a linear precoding system with a whitening transformation, makes PLC feasible in the FM band with an injected power spectral density (PSD) as low as -100 dBm/Hz (enough to avoid interference with FM signal reception systems).

Resumen

Los sistemas de comunicaciones por redes eléctricas, más comúnmente denotados con el acrónimo inglés *power line communication* (PLC), permiten el intercambio de información a través de cables eléctricos. Estos sistemas aprovechan la ubicuidad del cableado eléctrico ya desplegado para proporcionar acceso a servicios de telecomunicación sin necesidad de realizar ninguna instalación adicional. De hecho, una de las grandes ventajas de los sistemas PLC es su inmunidad al grosor de paredes y techos, lo que les permite tener un mayor alcance que las tecnologías inalámbricas en edificaciones con múltiples estancias y niveles.

Las aplicaciones PLC se pueden clasificar, atendiendo al escenario en el que se usan, en interiores y exteriores. Las aplicaciones exteriores suelen utilizar la red de distribución eléctrica por lo que las señales pueden viajar varios kilómetros de distancia. Una de las aplicaciones más extendidas de las PLC en exteriores son los contadores inteligentes. Por otro lado, las aplicaciones PLC en interiores suelen estar enfocadas a proporcionar mejores prestaciones de conectividad dentro de edificios. En ambos casos, los sistemas PLC pueden complementar los sistemas inalámbricos ampliando la cobertura alcanzada. Asimismo, los sistemas PLC también pueden clasificarse, conforme al ancho de bada utilizado, en sistemas de banda estrecha y sistemas de banda ancha. El trabajo presentado en este documento se enfoca en este último tipo.

Tradicionalmente, los sistemas PLC utilizaban sólo dos conductores, lo que da lugar a un sistema *single-input single-output* (SISO). Sin embargo, la mayoría del cableado que conforma las redes PLC interiores está compuesto por tres conductores en paralelo, por lo que este tercer conductor puede aprovecharse para habilitar un sistema *multiple-input multiple-output* (MIMO) sobre este canal, lo que puede aumentar notablemente las prestaciones alcanzadas. Las características de los canales MIMO se han estudiado ampliamente en entornos inalámbricos, pero los sistemas

MIMO sobre medios cableados muestran algunas diferencias con respecto a los inalámbricos. En particular, los canales que componen el enlace MIMO PLC muestran una relación más estrecha (mayor correlación espacial) que en el caso inalámbrico. Esta mayor correlación espacial puede observarse tanto en la respuesta del canal como en el ruido del canal PLC MIMO. En lo que respecta a la respuesta del canal, una mayor correlación espacial implica una menor ganancia de prestaciones MIMO, mientras que el ruido altamente correlado puede aprovecharse para lograr mayores ganancias de prestaciones MIMO. Sin embargo, se desconoce la dependencia de la correlación espacial del canal con la frecuencia (tanto de la respuesta del canal como del ruido), como también se desconoce la relación de la correlación espacial de la respuesta del canal con las características físicas de la red, como el tipo de cableado, el tipo de despliegue de la red (en árbol, en anillo), etc. Además, los modelos existentes de respuesta de canal MIMO no reflejan de forma realista la correlación espacial observada en las mediciones. Tanto los modelos PLC MIMO como las estrategias de transmisión deben tener en cuenta estas particularidades para sacar provecho de las capacidades MIMO que brinda el canal.

La primera contribución de este trabajo es un modelo MIMO PLC basado en líneas de transmisión multiconductor que refleja la correlación espacial de forma más exacta que los modelos previos. Para lograrlo, se proponen tres modificaciones en el modelo de canal que afectan a: cargas, ramas y cableado. El modelo propuesto proporciona canales MIMO similares a los medidos, tanto en términos de características de sus canales SISO individuales como en la correlación entre ellos.

La segunda contribución muestra, mediante medidas, que la correlación espacial en la respuesta del canal PLC no muestra una dependencia significativa con respecto a la frecuencia, al igual que en los escenarios MIMO inalámbricos, y que existen modos de inyección alternativos al diferencial habitual, como la inyección pseudodiferencial, que dan lugar a canales MIMO con una menor correlación espacial.

Por último, la tercera contribución proporciona una caracterización de la correlación del ruido en PLC MIMO en la banda de 2-108 MHz, donde se muestra que el ruido en la banda usada por la radiodifusión de FM (frecuencia modulada) presenta una correlación espacial muy elevada. Asimismo, se demuestra que el aprovechamiento de dicha correlación, mediante un sistema de precodificación lineal con una transformación de blanqueo, hace viable el PLC en la banda de FM con una densidad espectral de potencia inyectada de tan solo -100 dBm/Hz (lo suficientemente baja como para evitar interferir a los receptores de FM).

Contents

List of Acronyms

AM	**A**mplitude **M**odulation
AMR	**A**utomatic **M**eter **R**eading
ASK	**A**mplitude **S**hift **K**eying
AWGN	**A**dditive **W**hite **G**aussian **N**oise
BB	**B**road**B**and
bps	**b**its **p**er **s**econd
CDF	**C**umulative **D**istribution **F**unction
CENELEC	**C**omité **E**uropéen de **N**ormalisation **ELEC**trotechnique
CSMA/CA	**C**arrier **S**ense **M**ultiple **A**ccess/**C**ollision **A**voidance
DFT	**D**iscrete **F**ourier **T**ransform
DS	**D**elay **S**pread
DSL	**D**igital **S**ubscriber **L**ine
ETSI	**E**uropean **T**elecommunications **S**tandard **I**nstitute
EMC	**E**lectro**M**agnetic **C**ompatibility
EU	**E**uropean **U**nion
EV	**E**lectric **V**ehicle
EVSE	**E**lectric **V**ehicle **S**upply **E**quipment
FCC	**F**ederal **C**ommunication **C**ommission
FEC	**F**orward **E**rror **C**orrection
FM	**F**requency **M**odulation
FSK	**F**requency **S**hift **K**eying
G.hn	**G**igabit **h**ome **n**etworking
HDR	**H**igh **D**ata **R**ate

HF	**H**igh **F**requency
ICI	**I**nter **C**arrier **I**nterference
IEEE	**I**nstitute of **E**lectrical and **E**lectronics **E**ngineers
IoT	**I**nternet **o**f **T**hings
ISI	**I**nter **S**ymbol **I**nterference
ITU.T	**I**nternational **T**elecommunication **U**nion's **T**elecommunication Standardization Sector
LAN	**L**ocal **A**rea **N**etwork
LDPC	**L**ow **D**ensity **P**arity **C**heck
LDR	**L**ow **D**ata **R**ate
LF	**L**ow **F**requency
LPTV	**L**inear **P**eriodically **T**ime **V**arying
LTI	**L**inear **T**ime **I**nvariant
LV	**L**ow **V**oltage
MAC	**M**edium **A**ccess **C**ontrol
MF	**M**edium **F**requency
MIMO	**M**ultiple-**I**nput **M**ultiple-**O**utput
MTL	**M**ulticonductor **T**ransmission **L**ine
MV	**M**edium **V**oltage
NB	**N**arrow**B**and
OFDM	**O**rthogonal **F**requency **D**ivision **M**ultiplexing
PDF	**P**robability **D**ensity **F**unction
PHY	**Phy**sical layer
PLC	**P**ower **L**ine **C**ommunication
PRIME	**P**owerline **R**elated **I**ntelligent **M**etering **E**volution
PSD	**P**ower **S**pectral **D**ensity
PUL	**P**er-**U**nit-**L**ength
QAM	**Q**uadrature **A**mplitude **M**odulation

RCS	**R**ipple **C**arrier **S**ignaling
RV	**R**andom **V**ariable
SCR	**S**ilicon **C**ontroled **R**ectifiers
SISO	**S**ingle-**I**nput **S**ingle-**O**utput
SNR	**S**ignal-to-**N**oise **R**atio
SotA	**S**tate **o**f **t**he **A**rt
STF	**S**pecial **T**ask **F**orce
SVD	**S**ingular **V**alue **D**ecomposition
TDMA	**T**ime **D**ivision **M**ultiple **A**ccess
UDP	**U**ser **D**atagram **P**rotocol
UPA	**U**niversal **P**owerline **A**ssociation
USA	**U**nited **S**tates of **A**merica
UNB	**U**ltra **N**arrow**B**and
VHF	**V**ery **H**igh **F**requency
VLF	**V**ery **L**ow **F**requency

To those who have accompanied me during the toughest parts of this journey. I cannot thank you enough.

Chapter 1

Introduction

Over the past few decades, the telecommunication industry has experienced an exponential growth in both number of terminals and demanded data rate, mainly due to the ubiquity achieved by mobile networks, the Internet and the proliferation of concepts such as Internet of things (IoT). In order to satisfy the ever-growing demand, multiple solutions based on wired and wireless communications have been developed over the years. Specially remarkable from a usage standpoint are the local area network (LAN) standards Institute of Electrical and Electronics Engineers (IEEE) 802.3 [1] and IEEE 802.11 [2], commonly known as *Ethernet* and *Wi-Fi*, which define the medium access control (MAC) and physical layer (PHY) layers for wired and wireless LANs respectively. These two approaches have advantages of their own: while wireless LANs can provide easy coverage to a number of devices within a *large* zone, wired LANs attain faster and more reliable connections but has larger deployment cost. Power line communication (PLC) is a wired technology that features the inexpensive deployment of wireless ones, since it uses the ubiquitous power grid no new wires have to be deployed, while avoiding its coverage problems. However, the utility of PLC is not bound to LANs since throughout the years they have been widely used for multiple purposes, as it will be described in the following section.

1.1 Introduction to PLC

1.1.1 Historical overview

According to the early history of PLC as covered in [3], the idea of using power lines for signaling dates as back as to 1838 when Edward Davy proposed remote electricity supply metering for checking the voltage levels of batteries in the London-Liverpool telegraph system [4]. However, the first patent on a power line signaling electricity meter was not registered until 1897 by Routin and Brown [5].

In the 1930s, information was transmitted through ripple carrier signaling (RCS) in medium voltage (MV) (10-20 kV) and low voltage (LV) (240/415 V) distribution networks [6]. These systems used amplitude shift keying (ASK) and frequency shift keying (FSK) modulation schemes to carry digital information, although the low carrier frequency along with the simple narrowband modulations being employed caused the data rates to be quite low. Since then, many control and telemetry applications have been developed both for the *utility side*, as in the part involving equipment belonging to the utility company up to the domestic meter, and in the *consumer side*, involving equipment inside the consumer's premises. Regarding the latter, the first introduced applications included baby alarms, in the 1940s [7], and the home automation X10 protocol in the late 1970s [8]. With respect to the *utility side* applications, some of these may include automatic meter reading (AMR), remote connection, fraud detection and network management [9]. Additional applications for which PLC has been applied as a data transmission solution in both public and indoor electricity distribution networks can be found in [10].

The end of telecommunication monopolies in Europe in the 1990s stimulated the interest of utility companies in using their power distribution network to provide Internet access through PLC. This considerably encouraged the development of what can be referred to as first-generation broadband PLC systems, which achieved data rates of a few Mbit/s.

In the 2000s, the use of PLC as a last-mile technology lost momentum, as its performance was still poorer than the one offered by digital subscriber line (DSL) systems, while gained popularity as a technology for indoor local area networking. During this decade, the industrial alliances HomePlug and Universal Powerline Association (UPA) emerged, developing system specifications which can be referred to as second-generation and that featured bandwidths up to 30 MHz, orthogonal frequency-division multiplexing (OFDM) modulation, and data rates of tens of Mbit/s [11], [12].

In the 2010s, the standards International Telecommunication Union's Telecommunication Standardization Sector (ITU.T) gigabit home networking (G.hn) [13], IEEE P1901 [14] and the industrial specification HomePlug AV v2.1 [15] appeared. The defined systems, which can be referred to as third-generation, extend the bandwidth up to 80 MHz, include improved channel coding and multiple-input multiple-output (MIMO) techniques (except for the IEEE P1901, which is limited to 50 MHz and does not support MIMO). These result in maximum data rates of about 1 Gbit/s.

1.1.2 Classification of PLC systems

PLC systems can be classified according to diverse criteria. Following the categorization in [16], in this section we will focus on PLC systems regarding the application scenario and their bandwidth.

A common classification of PLC by application distinguishes between indoor, outdoor, and in-vehicle [10].

Indoor PLC is a heterogeneous group which comprises in-home PLC and industrial PLC.

- In-home PLC applies to residential environments and small offices. It is primarily used for applications such as smart home automation, energy management, home security systems, communication between smart devices and

local area networking within homes and small offices. Because of the latter, this scenario is also referred to as SOHO (small office-home office).

- Industrial PLC involves communication within industrial environments such as factories and industrial automation systems. It is mostly used to enable communication between sensors, actuators, motor drives and other industrial equipment.

Outdoor PLC is now mostly employed in Smart Grid and Smart City applications such as smart grid management, outdoor lighting control, AMR and outdoor surveillance systems. Many of the initial applications of PLC belong to this category, where PLC was used to communicate infrastructure components (monitoring systems, transformers and substations) and centralized management systems.

In-vehicle PLC has been repurposed from its initial application of enabling communication between the vehicle's control units, which is abandoned nowadays, to the communication between the electric vehicle (EV) and the corresponding electric vehicle supply equipment (EVSE). This allows negotiating charging sessions, including charging profile selection and payment.

PLC systems can also be categorized according to their bandwidth, as shown in Figure 1.1, as: narrowband (NB), medium frequency (MF) and broadband (BB)[1]. Figure 1.2 shows a summary of the main PLC standards and industrial specifications and their placement in the PLC bandwidth categorization.

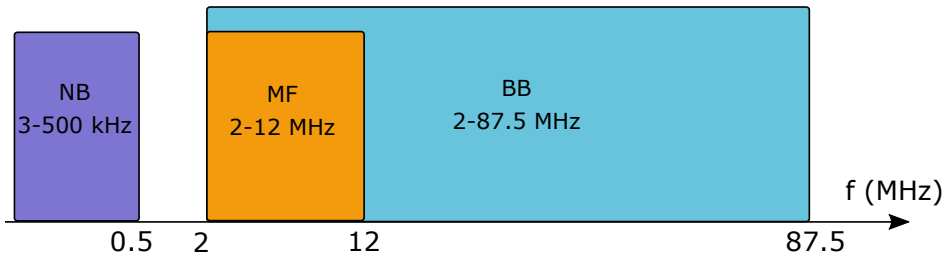

FIGURE 1.1: PLC system categorization according to its bandwidth.

[1]There is another category, apart from this three ones, called ultra narrowband (UNB) which usually takes place either in the ultra low frequency band (0.3-3 kHz) or in the upper part of the super low frequency band (30-300 Hz). It will not be covered in this work as it is not relevant for the purpose of this study.

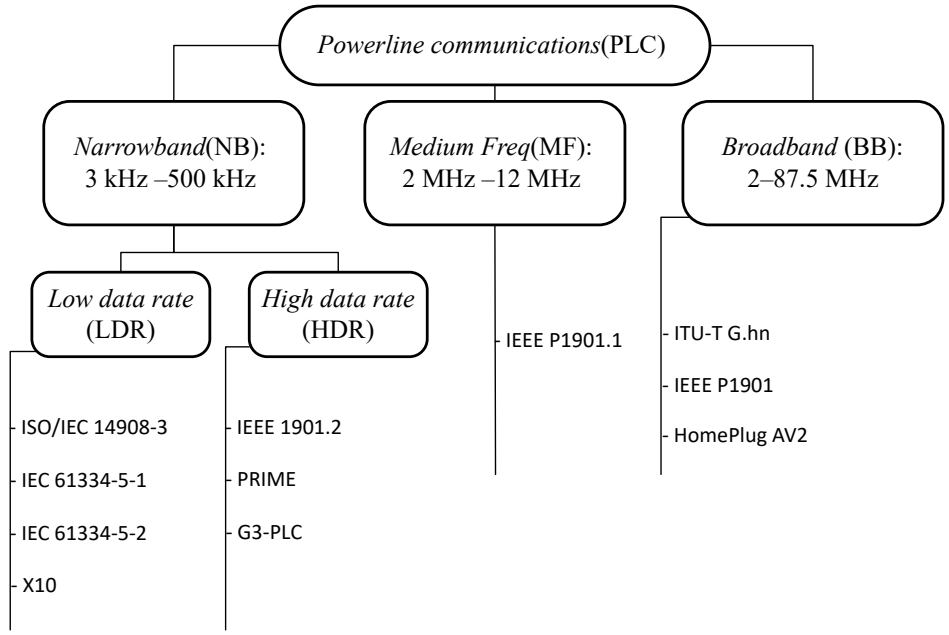

FIGURE 1.2: Noteworthy NB, MF, and BB PLC standards and industry specifications.

NB PLC comprises those technologies operating in the very low frequency (VLF)/low frequency (LF) bands (3-500 kHz). NB systems can be further arranged in the following categories according to their data rate: low data rate (LDR) systems use single carrier technologies (e.g., FSK) achieving data rates of few kbit/s and high data rate (HDR) systems use multicarrier technologies achieving data rates up to hundreds of kbit/s. NB PLC is being extensively used by utilities for AMR and home automation applications. Typical examples of LDR NB PLC technologies are those implemented according to the following recommendations: ISO/IEC 14908-3 (LonWorks) [17], IEC 61334-5-2 [18], and IEC 61334-5-1 [19], whose recommendations are widely deployed today by a number of companies, specially in Europe. Regarding HDR NB PLC, Powerline Related Intelligent Metering Evolution (PRIME) [20] and G3-PLC [21], specify solutions based on OFDM operating in frequencies up to 490 kHz which have gained gained industry support in Europe.

The term MF PLC refers to systems complying with the IEEE P1901.1 standard [22], which use the frequency band 2-12 MHz and that are targeted at Smart Grid

and IoT applications. Systems complying with this standard use OFDM and convolutional turbo coding, achieving data rates of about 4 Mbit/s and up to 1 km per hop with up to 15 levels of repeaters [23].

BB PLC operates in the high frequency (HF)/very high frequency (VHF) bands (1.8-250 MHz). State-of-the-art systems employ multicarrier modulations (OFDM and wavelet OFDM), strong forward error correction (FEC) schemes, time division multiple access (TDMA)-based MAC with contention-free and carrier sense multiple access/collision avoidance (CSMA/CA) regions and, in most cases, MIMO technology. This allows achieving maximum data rates of up to 1 Gibt/s (although values in actual scenarios are in the order of hundreds of Mbit/s). They are widely used in indoor scenarios for LAN applications, although they are also used in Smart Grid applications for connecting secondary substations and also for AMR. The most relevant BB PLC standards are ITU.T G.hn [24], and IEEE P1901 [14], whereas the most relevant industry specification is HomePlug AV2 [15].

This thesis is focused on indoor BB PLC, hence, the information provided in the following sections refers to channels in this scenario, unless stated otherwise.

1.1.3 Channel response and noise

Power lines were not conceived for communication purposes but to deliver electrical energy, which involves a very different kind of signals regarding frequency and power. Hence, it is not surprising that the PLC medium is an adverse medium for communication signals. This section summarizes the main features of the PLC channel response and noise.

In most countries, in-home power grids exhibit a tree-like layout consisting of multiple circuits deployed from the main panel to the outlets and luminaries. Each circuit typically consists of three conductors: phase, neutral and protective earth. Since cables are electrically long at the frequencies of the communication signal, a multipath propagation phenomenon occurs due to the reflection at the branches and

the impedance mismatch at the cable joints, connected devices, light switches and outlets. This yields a frequency selective channel response in which the resulting attenuation profile depends on several factors: the network topology, the direct path followed by the signal from transmitter to receiver and the connected loads. In fact, the length of the direct link between transmitter and receiver might not be the most relevant feature since it is common for a shorter link to present larger attenuation than a longer one [25]. Moreover, the coherence bandwidth of the channel is higher at higher frequencies, where the increased attenuation (mainly due to the skin effect) reduces the influence of the reflected terms.

The response of indoor BB PLC channels also exhibit a twofold time variation. One is due to the connection and disconnection of electrical to the indoor power grid. Since these changes usually occur in the order of minutes or hours, which is much lower than the symbol rate typically employed, they are usually referred to as long-term changes [25]. The other time variation is due to the non-linear behavior of the electrical devices connected to the network. When excited with the sum of a low frequency and high level signal (the mains one) and a high frequency and low amplitude one (the communication signal), the resulting effect can be modelled as periodically time-varying impedance synchronized with the mains. This causes a short-term variation of the channel response, which can be modelled as a linear periodically time-varying (LPTV) system. Fortunately, the channel is underspread, as the impulse response is shorter than the coherence time of the channel [26]. In practice, the short-term variation of the channel response is usually located below 20 MHz and the linear and time-invariant (LTI) assumption is made.

Indoor BB PLC noise does not follow the classical additive white Gaussian noise (AWGN) model. It has two main origins: noise generated by the electrical devices connected to the power grid and external noise coupled to the indoor network via radiation or via conduction. Indoor PLC noise can be decomposed in the following components [27]:

- Impulsive noise, which in turn is comprised of periodic impulsive noise synchronous with the mains, periodic impulsive noise asynchronous with the mains, and sporadic impulsive noise. The former typically consists of large amplitude and duration impulses with a frequency equal or twice the one of the mains signal (e.g., 50/100 Hz in Europe). The latter consists of isolated impulses, or train of impulses, that appear at random. Finally, the periodic impulsive noise asynchronous with the mains takes the form of impulse trains that always appear at the same instants of the mains cycle but in which the repetition rate of their constituents impulses is not related to the mains frequency.

- NB interference. It generally consists of sinusoidal or modulated signals originated by broadcast stations that are coupled via radiation. Its level usually varies along the day and can be modelled as a cyclostationary process and, in some cases, as a stationary one. They are typically located below 30 MHz.

- Background noise. This includes all the noise that has not been included in the previous categories. It can be assumed to be cyclostationary and its level depends on the number and type of electrical devices connected to the network. Since it usually results from the contribution of multiple noise sources, the Gaussian assumption is generally valid.

1.1.4 Standards and EMC regulations

This section briefly reviews the BB PLC communication standards and industry specifications and the electromagnetic compatibility (EMC) regulations they have to comply with.

BB PLC systems with highest performance currently found in the market are designed according to the ITU.T G.hn and IEEE P1901 standards and the HomePlug AV2 industry specification [24][14][15], which were developed about one decade ago. They all use multicarrier modulations and TDMA-based MAC with both a

connection oriented, contention-free service, and a connectionless service based on CSMA/CA. They are not interoperable, although coexistence mechanisms have been defined.

The ITU.T G.hn is the term used to refer to a set of ITU.T Recommendations of the G series (which addresses transmission systems and media, digital systems and networks) for home networking over different transmission media (telephone wiring, coaxial cables, power lines, and plastic optical fiber). ITU.T G.hn includes the following Recommendations: G.9960 (physical layer and network architecture) [28], G.9961 (data link layer) [29], G.9962 (management), G.9963 (MIMO) [13], G.9964 (power spectral density (PSD)) [30] and G.9972 (coexistence) [31].

ITU.T G.hn defines a pulse-shaped OFDM-based system with 4096 carriers in the frequency band up to 100 MHz[2]. Quadrature amplitude modulation (QAM) constellations of up to 12 bits/symbol are employed. Low-density parity-check (LDPC) coding with different coding rates are used. It supports MIMO of up to 2×4, although the 2×3 is the most widely used. These allow achieving data rates up to 1 Gbit/s at user datagram protocol (UDP) level and up to 1.5 Gbit/s at the physical layer.

The IEEE P1901 standard defines two non-interoperable physical layers working in the frequency band up to 50 MHz, one based on OFDM and the other on wavelet OFDM [14]. The former employs 2048 carriers while the latter uses 1024. The FEC of the OFDM-based system uses turbo coding, while the one of the wavelet OFDM concatenates a Reed-Solomon and a convolutional code. A drawback of the IEEE P1901 with respect to the ITU.T G.hn is that MIMO is not supported. However, it defines a specific architecture for Smart Grid outdoor applications. The maximum data rate at the physical layer is about 500 Mbit/s.

HomePlug AV2 is an industry specification developed by the HomePlug Powerline Alliance (now without activity) [15]. It defines a pulse-shaped OFDM-based

[2]The actual frequency is limited by EMC regulations to 80/86 MHz, depending on the region, as described below.

system with 4096 carriers in the frequency band up to 100 MHz[2]. Like the ITU.T G.hn, it also uses QAM constellations with up to 12 bits/symbol but a turbo coding is used for FEC purposes instead. The exploitation of MIMO techniques allows it to achieve a maximum physical data rate of about 1.5 Gbit/s.

Table 1.1 summarizes the main physical layer parameters of the three presented systems.

Parameter	**ITU.T G.hn**	**IEEE P1901 OFDM | wavelet**	**HomePlug AV2**
Frequency band (MHz)	100	50	100
Number of carriers[(a)]	4096	2048 | 1024	4096
Intercarrier spacing of the header and data carriers (kHz)	24.414	24.414 | 47.07	24.414
Min–max guard interval (μs)	1.28–10.24	1.6–47.12 | -	0–47.12
Rolloff interval (μs)	5.12	4.96 | -	4.96
Max number bits per symbol	12	12|5	12
Coding rates	1/2, 2/3, 5/6, 16/18, 20/21	1/2, 16/21, 16/18 | $[\frac{40}{56}, \frac{239}{255}] \times \frac{k}{k+1}$ [(b)]	1/2, 16/21, 16/18
MIMO[(c)]	2×3	-	2×3

[(a)] The number of active carriers is actually lower and determined by the electromagnetic compatibility regulations indicated below.

[(b)] Two possible Reed-Solomon rates and convolutional code with $k = 1, \ldots, 7$.

[(c)] Typical values, but up to 2×4 could be employed.

TABLE 1.1: Summary of the main physical layer parameters of the the ITU.T G.hn, IEEE P1901 and HomePlug AV2 [32].

The previous standards/specifications are designed to comply with current EMC regulations, as summarized in Figure 1.3. These regulations define the frequency band that can be employed by PLC systems and the maximum level of the injected

or radiated signal. A brief summary of the regulations issued by the Comité Européen de Normalisation Électrotechnique (CENELEC) and the Federal Communication Commission (FCC) will be provided below. The reader is referred to [33]–[35] for a comprehensive description of the regulations concerning both NB and BB PLC.

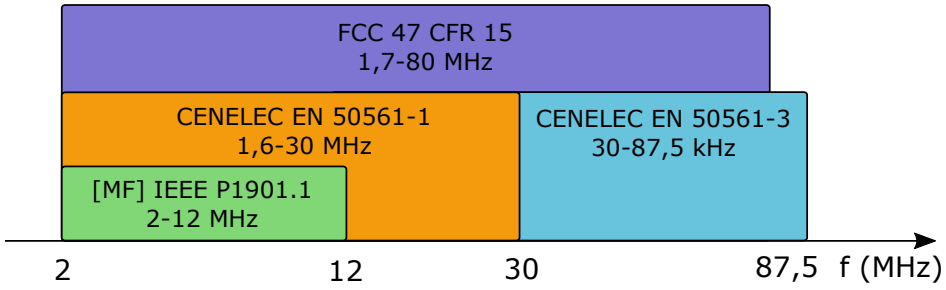

FIGURE 1.3: Medium and Broadband PLC regulatory frequency bands.

In the European Union (EU), in-home single-input single-output (SISO) PLC (note that MIMO are not included) systems have to comply with the EN50561-1 [36] in the frequency band from 1.6065-30 MHz and with the EN50561-3 [37] in the range 30-87.5 MHz. The former only defines a set of permanent and dynamically excluded sub-bands to avoid interfering existing systems, but no limits to the injected signal is imposed, as it is done in the latter. Systems defined according to the ITU.T G.hn have to comply with the ITU.T Recommendation G.9964, which allows the injected signal to have a PSD of -55 dBm/Hz in the range 2–30 MHz and -85 dBm/Hz in the range 30–80 MHz.

Outdoor BB PLC is not regulated by an harmonized standard in the EU, as the EN-50561-2, which is aimed at regulating these systems has been under discussion for a long time. This situation also applies to MIMO (both in-home and outdoor) systems. Deployed systems rely on the EU Directive 2014/30/EU, which allows manufacturers to issue a Declaration of Conformity (DoC) in which they carry out the EMC assessment (aimed at proving that their systems cause no interference to existing systems) based on its own procedures.

In United States of America (USA) both indoor and outdoor BB PLC are allowed

to use the 1.705-80 MHz band, as regulated by the FCC under Code of Federal Regulations, Title 47, Part 15 [38]. This regulation sets limits to the radiated emissions, which have been differently translated to limits in the PSD of the injected signal, e.g., -50 dBm/Hz in the 1.8–30 MHz range and -80 dBm/Hz in the 30–86 MHz band are proposed in [39], which are quite similar to the limits set by the ITU.T G.9964.

1.2 MIMO PLC

MIMO is a method for enhancing the performance of a link using multiple transmission and receiving endpoints to exploit multipath propagation. This strategy is widely used in wireless communication systems where multiple antennas, both at the transmitter and receiver end, can be used as a diversity technique, to improve error probability, and as a multiplexing strategy, to increase data rate. The former is referred to as MIMO beamforming and the latter as MIMO multiplexing [40]. In both cases, full potential gain is obtained when each antenna receives an uncorrelated version of the transmitted signals. Conversely, the benefit reported by MIMO techniques is maximum when captured noise is fully correlated among all ports.

MIMO PLC exploits the presence of three wires (phase, neutral and protective earth) in most indoor power networks. At the transmitter side, two differential voltage signals can be injected between pairs of wires since, according to Kirchoff's law, only two independent differential signals can be injected using three wires[3]. At the receiver side, the three differential paths show some diversity. Hence, differential signals between the three conductors (generally named PN, NE and EP can be obtained) or between each conductor and a reference voltage obtained from the transformer used in the coupling circuits can obtained. Moreover, a common mode (CM) signal can be also obtained if a large metal plate is available (e.g., as in large TV).

[3]These three conductors are usually known as P (phase), N (neutral) and E (earth)

Full MIMO potential gain is not achievable in many situations since the channel responses between each pair of transmitting and receiving ports are usually correlated, which reduces the gain achievable by MIMO techniques. Since correlation between the channel responses in wireless scenarios is strongly determined by the distance between antennas, the term spatial correlation is employed to denote this phenomenon. Unfortunately, spatial correlation in MIMO PLC links is typically larger than in their wireless counterparts, which reduces the MIMO gain. This MIMO PLC channel correlation is determined by the characteristics of the underlying power network, as it is shown in [41] and [42] which can be found in Chapter 3.

On the other hand, noise correlation improves the performance of MIMO systems, since received noise in a given receiving port can be used to cancel out noise in the remaining ones, yielding a virtually noise-free channel. Fortunately, noise correlation in MIMO PLC is larger than in wireless environments, where the received noise in each receiving port can be assumed to be independent. Therefore, noise correlation in MIMO PLC systems improves their performance, as discussed in [43] in Chapter 3.

In the following, a brief summary of the main published works related to MIMO PLC is given.

MIMO PLC Channel Measurements. An introduction to the fundamentals of MIMO PLC can be found in [44]. This work proposes a measurement setup whose results motivated to implement a MIMO PLC feasibility study in hardware. The following year, the work in [45] described the field measurement campaign carried out by the European Telecommunications Standard Institute (ETSI) Special Task Force (STF) 410 , which comprised six European countries and covered the 0-100 MHz range, whose goal was to verify the feasibility of MIMO PLC.

Channel spatial correlation analysis. A deep dive on the channel response obtained by the ETSI STF 410 can be found in [46]. This paper provided an estimation of the MIMO system performance over the channels measured by the STF 410 and found out that the spatial correlation of the channels yielded a second MIMO

stream 15 dB weaker on roughly half the frequencies under study. However, this analysis did not make any distinction among frequency bands. The analysis in [47], performed over 96 channels captured from five dwellings in North America, takes into account different frequency bands but measured channels are registered using HomePlug AV receivers. Hence, obtained results are conditioned by the system parameters. None of this works covered the influence that the electrical appliances or other components of the electrical network may have on the spatial correlation.

Noise correlation (time and spectral-wise). Whereas [46] focused on the channel analysis from the STF 410 measurements, its noise counterpart can be found in [48]. One of the most interesting contributions of this work is that it showed the strong time domain correlation present on the receiving ports. On the other hand, [49] studies the noise spatial correlation on the same North American measurements covered in [47]. However, the statistical analysis in [49] does not discriminate by frequency bands even though there is strong evidence that there is indeed dependence between noise spatial correlation and the noise frequency band under analysis. Moreover, as indicated above, the measurements were obtained by receivers HomePlug AV2 compliant, therefore they are biased by the technical specification settings.

MIMO channel response model. Although field measurement campaigns, such as the ones described above, are a key part of the MIMO/SISO PLC system development, the development of accurate channel models is equally as important. As a rule thumb there are two approaches to build a PLC channel model: the bottom-up model, which aims to replicate the underlying structure of the channel[4] by modeling the deployed cables as a set of interconnected multiconductor transmission line (MTL), and the top-down model, where the channel response is modelled by a mathematical expression whose parameters are determined to match a set of measured channel responses. Regarding bottom-up PLC models, the idea of using MTL

[4]This is done under the premise that if the underlying structure is correctly defined, the model response should be quite similar to the real scenario it mimics.

theory to estimate the response of PLC channels was proposed in [50]. However, the purpose of [50] was to measure the effect of the ground wire on the SISO channel response, it was not an attempt to provide a MIMO channel model as such. This was proposed in [51] where MTL was applied to get the channel response of MIMO links. However, the modeled channels in [51] yielded an artificially symmetric MIMO channel response, which in turn implied that the spatial correlation was invariant with respect to frequency. This result was not realistic according to the analysis in [47]. Regarding top-down models, the most popular approach is the "echo-based" model, first introduced by [52] and refined in many later works such as [53] and [54]. A thorough review of the State of the Art on PLC channel modelling is provided in Chapter 2.

PLC system performance. The performance of MIMO PLC systems was explored in works as early as [44], where the authors modeled noise as a white Gaussian process, which is somewhat unrealistic. Under this assumption, it was revealed that the average channel capacity of the 2×4 MIMO configuration was twice the SISO's, and at the 98% coverage point a simpler system (2×2) showed double the performance of a SISO one. That gain could grow up to a factor of 2.6 when a 2×4 configuration was employed instead of the 2×2. Lastly, the effect of noise spatial correlation on the performance of a MIMO PLC system is evaluated in [55]. This analysis was carried out taking into account frequencies below 86 MHz and it was shown that the performance improvement that could be obtained from exploiting the noise spatial correlation was quite low.

1.3 Objectives and outline of the thesis

1.3.1 Objectives

This thesis focuses on indoor broadband PLC systems. In this context, its **main objective** is to study MIMO PLC channels, focusing on the differentiating factors

from other environments, such as spatial and noise correlation, and to develop a MIMO PLC channel model and an associated channel generator. To this end, the following partial objectives have been defined:

- **Analysis of the spatial correlation of MIMO PLC channel response**. The study is aimed at assessing the influence of the frequency, the wiring of the underlying network and of the employed injection method on the spatial correlation. The former is important for the development of top-down MIMO PLC channel models, specially those in which the channel is modelled as a multivariate random variable whose covariance matrix has to reflect the relation between the MIMO paths at all frequencies. Regarding the cabling employed in indoor power grids, since it varies among countries (some use monopolar cables while other use multipolar ones), it is important to analyse its influence in the spatial correlation, as it may notably influence the performance of MIMO systems. In the aforementioned analysis, the MIMO coupling circuit is considered as part of the channel, however, since different circuits have been proposed in the literature, it is interesting to assess their influence in the spatial correlation.

- **Development of a MIMO PLC channel response model and a corresponding simulator**. This task can be split in two objectives:

  - Development of a bottom-up MIMO PLC channel response model. An appropriate channel model is of paramount importance of the design and performance assessment of transmission techniques. MIMO bottom-up models based on MTL are the natural extension of the models already employed for SISO channels. The model proposed in [56] follows this strategy, however, it fails to reflect the relationship that exists between the responses of the MIMO paths, yielding channels with unrealistically similar MIMO streams. We conjecture that this lack of realism is due to the asymmetries of the network (e.g., derivations to the luminaries), which

are not reflected in the referred model. Hence, the aim of this task is to identify the asymmetries of the indoor power grid with larger influence in the spatial correlation and to propose adequate models that can be included in the developed MTL-based channel model.

  - Implementation of a MIMO PLC channel response simulator. This task is aimed at extending an existing bottom-up SISO channel simulator (developed by the PLC group of the Departamento de Ingeniería de Comunicaciones of the Universidad de Málaga) in two ways. First, by modeling the cabling using tree-conductor transmission lines and, second, by adding a random topology generator that allows obtaining realistic indoor power networks.

- **Study of the noise correlation in MIMO PLC systems.** Noise correlation in MIMO PLC systems has already been analyzed in the whole 2-88 MHz band. However, we conjecture that noise correlation should have a strong dependency with frequency, since radiated emissions from distant sources coupled to the indoor power network should be more prominent at high frequencies than at low ones. This phenomenon would be particularly important in the 88-100 MHz band, which in most countries is assigned to frequency modulation (FM) broadcasting services. Hence, this task is aimed at analyzing noise correlation in different frequency bands, in particular in the FM one, and to assess the data-rate that can be attained by exploiting this phenomenon by means of a whitening transformation.

1.3.2 Outline of the thesis

In this chapter, a historical overview of PLC has been given along with the main goals of the work. Chapter 2 gives a thorough review of the state-of-the-art in PLC, focusing on MIMO aspects. Chapter 3 includes a copy of the publications that have been produced as a result of the conducted research. Finally, general conclusions

drawn from this work are summarized in chapter 4 along with suggestions for further study.

Due to space limitations, relevant aspects of one of the papers presented in Chapter 3, [41], could not be covered in such publication. For the sake of completion, the analytical MTL expressions used in [41] are summarized in Appendix A, and the steps taken to validate the implementation of such expressions are shown in Appendix B.

Chapter 2

Characterization and modelling of indoor broadband PLC channels

This chapter describes the current state of the art of indoor broadband MIMO PLC noise and channel response characterization and modelling. Since a MIMO PLC channel is actually a related set of SISO channels, the first part of this chapter provides insight on the features of SISO PLC channels. The second part of this chapter focuses on the characterization and modelling of the response of MIMO channels, while the third one covers MIMO PLC noise.

2.1 SISO PLC channel response and noise features

2.1.1 SISO PLC channel response characterization and modelling

Channel characterization

Indoor power networks typically have a tree-like layout in which circuits are deployed from the main panel to the outlets and luminaries, as depicted in Fig. 2.1. As a result of the notable differences in topology and cabling, PLC channels notably differ from conventional wired media using twisted pair and coaxial cables, presenting rather hostile properties and exhibiting some typical properties from wired ones (determinism) but also from wireless channels (time variation).

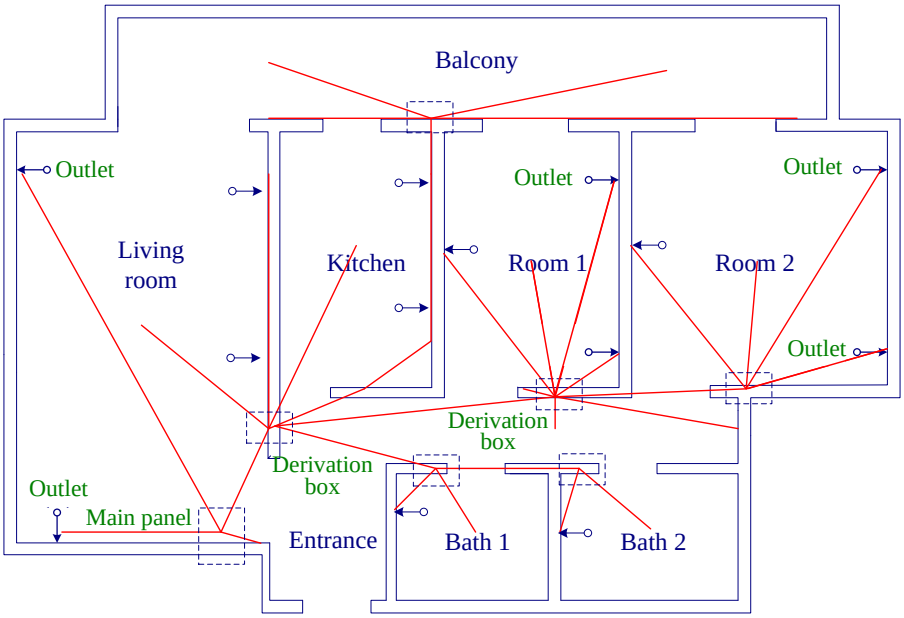

FIGURE 2.1: Illustrative example of an indoor power grid layout. Adapted from [57].

Since cables are electrically long at the frequencies of the communication signal, reflections occur due to impedance mismatch at joints causing a multipath propagation phenomenon that yields a frequency selective channel response [52], [58]. Fig. 2.2 illustrates this end by depicting the amplitude response of three indoor measured channels in the frequency band up to 80 MHz: one with low attenuation, one with intermediate attenuation and a highly attenuated one. In order to highlight the differences between indoor and outdoor channels, it also shows the amplitude of two representative modeled outdoor channels corresponding to links with approximate lengths of 76.2 m (which is in the order of a long indoor link) and 216 m. In outdoor channels, the frequency selectivity associated to the multipath propagation is generally less important, as it is masked by the larger attenuation resultant from the skin effect, yielding amplitude responses with the low-pass profile shown in Fig. 2.2.

Attenuation and frequency selectivity are generally correlated effects, meaning lowly attenuated channels tend to have "flatter" amplitude responses (i.e., having larger coherent bandwidth), as illustrated in Fig. 2.3, which depicts a scatter plot of

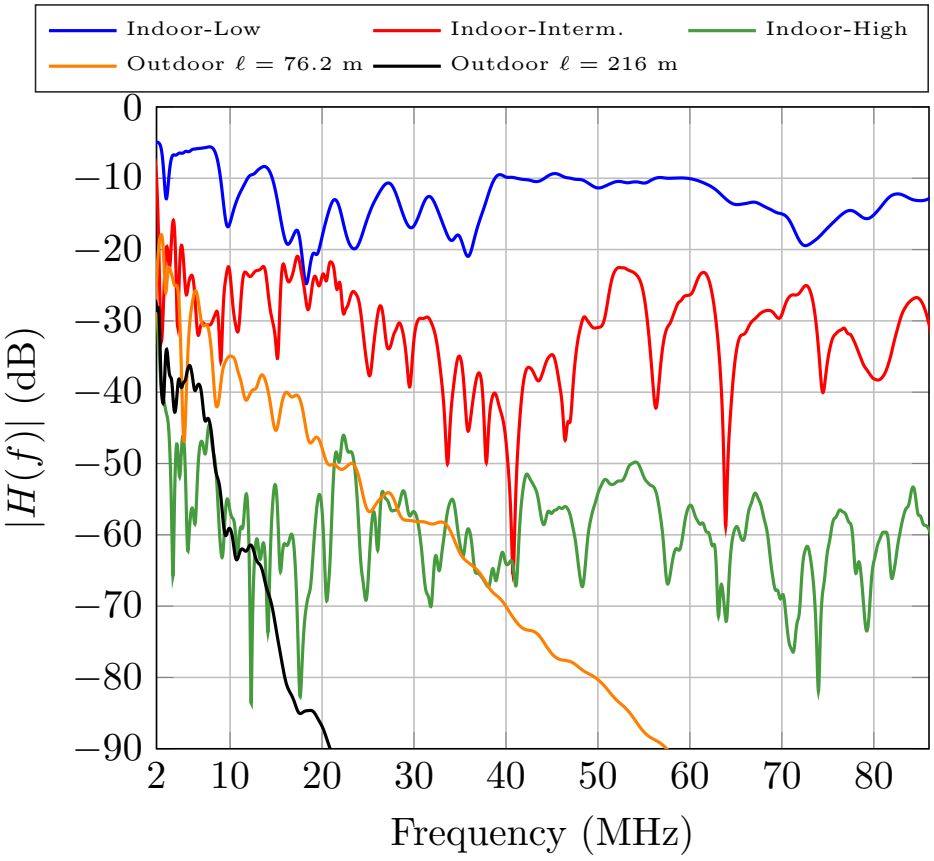

FIGURE 2.2: Amplitude response of three measured indoor channels and two representative outdoor modeled ones.

the coherence bandwidth vs the average amplitude response of a set of measured channels. This phenomenon has different causes in the low and high frequency regions. In the 1–30 MHz range, attenuation is mainly due to the notches caused by the multipath propagation phenomenon. Channels corresponding to longer links will have more derivations from the main path from the transmitter to the receiver than shorter ones. These derivations result in a larger number of notches that increase the attenuation and reduce the coherence bandwidth. In the 30–86 MHz band, the skin effect becomes relevant, causing longer links to have more pronounced low pass behavior and lower coherence bandwidths.

The impulse response of indoor PLC channels consists of a very large number of delayed echoes that result from the potentially infinite number of forward and backward-traveling waves that result from the reflections caused by impedance mismatch at cable junctions, open circuits and at the electrical devices connected to the

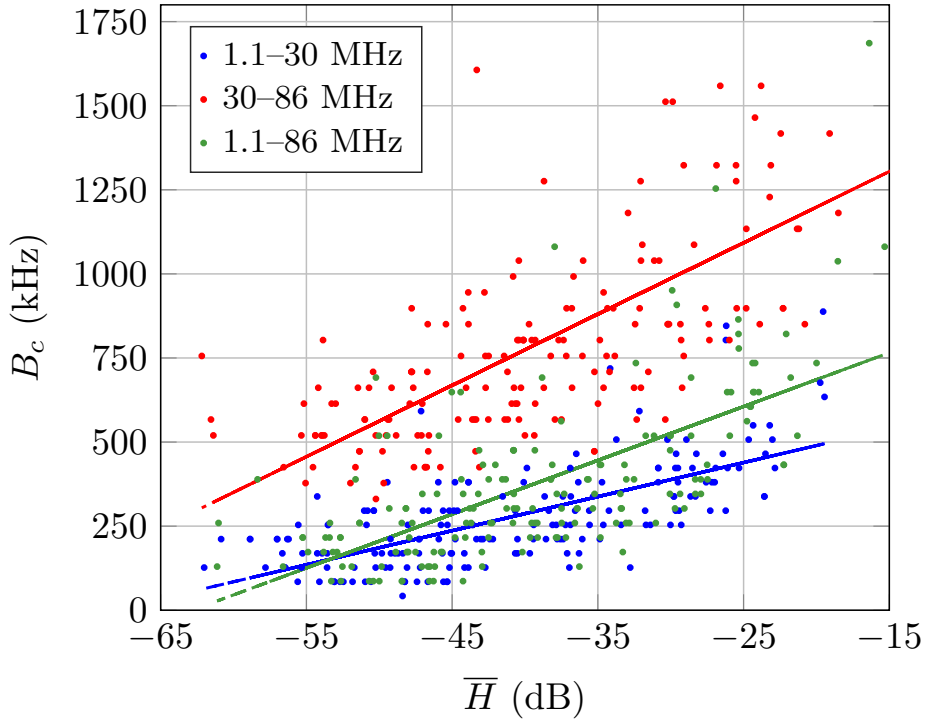

FIGURE 2.3: Scatter plot of the coherence bandwidth against the average amplitude response of measured indoor channels, [59].

power network. This contrast to wireless channels, which can be generally modelled using a relative low number of echoes. The impulse response length is conventionally quantified by means of the delay spread (DS). In indoor PLC scenarios, it has been shown that the relation between the DS and the coherence bandwidth can be modeled using a hyperbolic relation, as illustrated in Fig. 2.4.

As stated in the Introduction, PLC channels exhibit long-term and short-term time variations. From a communications perspective, only the latter are relevant, as the rate of the former is much longer than the symbol periods typically employed. However, short-term variations tend to be located in the low frequency band, as illustrated in Fig. 2.5a, where the time variation along the 20 ms of the mains cycle of the amplitude response of a channel measured in Spain in the frequency band up to 20 MHz is depited and in Fig. 2.5b, which details the evolution of the amplitude response at two frequencies. Since the channel is underspread, the LTI assumption is generally accepted.

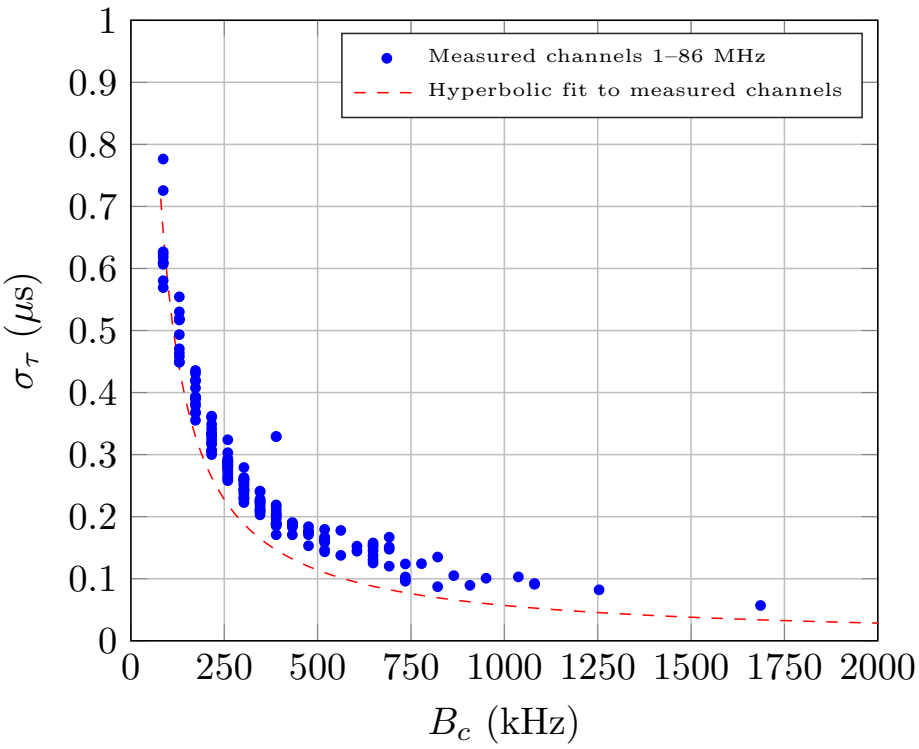

FIGURE 2.4: Scatter plot of the DS vs the coherence bandwidth of measured indoor channels along with its hyperbolic approximation. Adapted from [60].

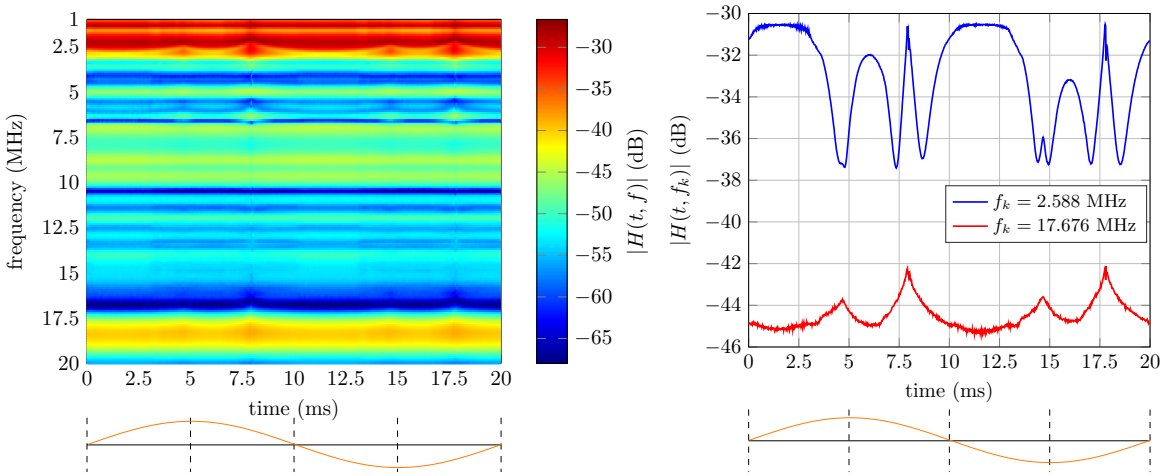

(A) Spectrogram of the amplitude response

(B) Time variation of the amplitude response at two frequencies

FIGURE 2.5: Illustrative example of the short-term variation of the amplitude response of a measured channel along the mains period. Adapted from [61].

Channel modelling

PLC channel response modelling strategies can be classified into three categories, as illustrated in Fig.2.6: top-down, bottom-up and machine learning-based. A brief

description of each approach is given below, except for the latter [62], which is still in a too embryonic state and will not be considered here.

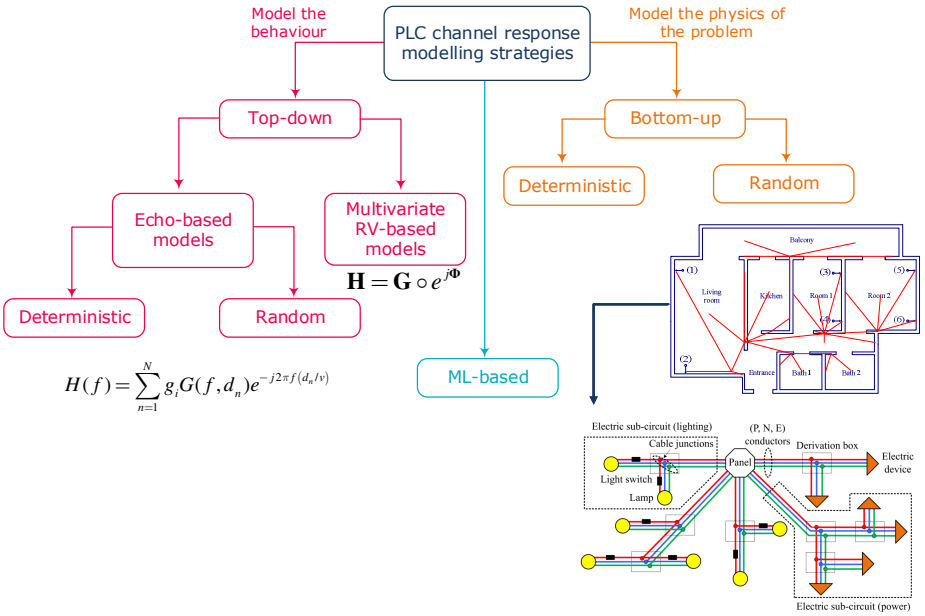

FIGURE 2.6: Categorization of PLC channel response modelling strategies. Adapted from [60].

Top-down models can be categorized into two groups: echo-based models and multivariate random variable (RV)-based models. The former models the channel response as a set of delayed echoes whose parameters are derived from measurements. These parameters can be randomly varied, according to statistics derived from measurements, or fixed to match some reference channels or group of channels. Models based on this approach were proposed in [63] for indoor scenarios in the frequency band up to 30 MHz and for outdoor ones in the band up to 20 MHz in [52].

The Opera project, funded by the EU Commission, proposed top-down models for both outdoor channels of frequencies up to 20 MHz and for indoor ones of frequencies up to 50 MHz [64]. Three reference outdoor channels are defined and the parameters of an echo-based model that provides the best fit are given. However, a more heuristic approach is proposed for indoor channels.

In order to assess the performance of communication systems, a large number of statistically representative channels are required. To this end, the work in [53] proposed a set of probability distributions for the parameters of the model in [52]. However, the proposed distributions are not empirically supported.

An important milestone in the development of top-down models is the observation that the average channel gain and the DS can be assumed to be log-normally distributed, which is exploited to obtain a simple two-tap echo-based model [54][65].

While echo-based models with a relatively low number of echoes can be suitable to model outdoor PLC channels, a much larger number is required for indoor channels. This is due to the potentially infinite number of forward- and backward-traveling waves that appear because of the reflections caused by impedance mismatch and that reach the receiver much less attenuated than in outdoor scenarios. Consequently, models of this type proposed in the literature are unable to replicate key features of indoor PLC channels, such as the relation between the DS and the average attenuation [66].

The work in [67] proposes a top-down model which is not based on a set of delayed echoes. Measured channel responses are classified according to its average attenuation into 9 classes. Modeled channels are generated by randomly adding peaks and notches to the average channel response of each class.

In the multivariate RV-based approach the amplitude and phase of the frequency response are modelled as multivariate RVs. Published works model the amplitude of the channel frequency response as a log-normal multivariate RV [68], [69]. While this assumption is still controversial, as some reported measurements support this end [70] but others do not [56], it seems to be the one that yields the best fit among the proposals that have been tested. The work in [68] assumes that the correlation matrix of the amplitude response depends only on the frequency lag, which overestimates the coherence bandwidth in the high frequency band, where the amplitude response is less frequency selective than in the low frequency range because the

multipath propagation phenomenon is less severe as the reflected waves reach the receiver more attenuated. A model that takes this into account has been proposed in [69].

It is worth noting that the popularity of top-down models (typically used in wireless scenarios) have caused the misconception that there is fading in PLC channels. Thus, it is common to find in the literature works in which the response of a PLC channel at a given frequency is assumed to experience an ergodic fading process which commonly follows a log-normal distribution (although the Rayleigh one is also used). This misunderstands that randomness in PLC channels is associated to the topology of the network under consideration and to the location of the transmitter and receiver within it. This yields a non-ergodic behavior that contrasts to wireless links, where the channel between all pairs of transmitter and receiver locations undergo the same fading states, although in different time order. Hence, the log-normal assumption in PLC should be applied to the ensemble of all PLC channels, i.e., for all possible pairs of transmitter and receiver positions and network topologies, but the channel is deterministic once the transmitter and the receiver are placed (except for long-term changes).

The following list summarizes advantages and drawbacks of the top-down modelling approach:

- Advantages:
  - They are useful to generate statistically representative channels.
  - The underlying distributions used in their definition are useful for developing optimum techniques for signal transmission and reception.
  - Generating channels is simpler than with bottom-up models.
- Drawbacks:
  - They are unable to infer the channel responses in a given PLC network.

– It is hard to account for changes in the channel response, specially short-term ones.

Bottom-up models rely on the physical description of the considered power network, which is modelled by means of transmission line theory. Bottom-up models were firstly proposed for outdoor MV and LV lines [71][72] for frequencies below 100 kHz and in [73] for frequencies up to 30 MHz. Interestingly, since MV and LV distribution networks use three-phase wiring, the works in [71] and [73] employed an MTL approach.

The first bottom-up models for indoor PLC channels in the frequency band up to 30 MHz disregarded the protective earth conductor and modeled the power network as a set of interconnected two-conductor transmission lines [74], yielding a SISO channel model. They also disregard the asymmetries in the network due to the light switches (where the phase conductor reaches the luminary by way of the switch, while the neutral conductor is directly deployed) and assumed a constant separation between conductors (which does not hold when monopolar cables are employed). Despite the uncertainties in the topology and characteristics of the underlying network, these models yield a good fit for measured channels [25].

Long-term changes in the channel were modeled by changing the impedance of the loads connected to the network following a Markov Process [25]. In [26], short-term variations synchronous with the mains (mainly located in the frequency range below 20 MHz) are added into the model, applying slow-variation approximation[1], via LPTV models consisting of LTI states.

The aforementioned models rely on a description of the topology of the considered power network and the characteristics of the employed cables. However, bottom-up models can be also used to generate large sets of statistically representative channels by generating random topologies. To this end, [75] introduces a simple topology consisting of a main path from the transmitter to the receiver and three derivations, where the length of the lines and their attached loads are randomly

[1]Changes are way slower that the channel impulse response length.

generated, as shown in Fig. 2.7. The simplicity of the considered network calls for an artificial increase of the attenuation of the considered conductors to match the average channel attenuation of the actual channels. However, this makes the generated channels to have an unrealistic low-pass profile. The work in [76] proposes a random topology generator which gives more realistic networks at the cost of increased complexity. To this end, a layout of the indoor premise is firstly generated by dividing the area of the premise into a number of random clusters (rooms) of square shape with identical area. A derivation box is placed in each cluster from which cables to the outlets are deployed either in a start structure or in a bus one.

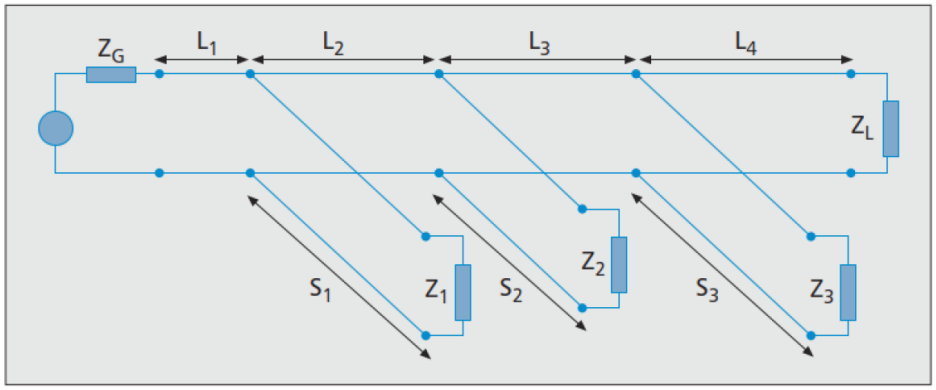

FIGURE 2.7: Simplified three-derivation topology proposed in [75] for bottom-up modelling of PLC channel responses. Figure extracted from [75].

The referred works model the network using two-conductor transmission line theory, which disregards the influence of the protective earth conductor in the SISO channel established between the phase and neutral conductors. However, the work in [50] highlighted that the effect of the protective earth is not negligible when grounding practices like bonding (the protective earth and the neutral conductor are connected at the main panel via a low resistor), typically used in North America, are employed. To take this into account, [50] models the indoor network using MTL.

Similarly to the top-down approach, the bottom-down approach carries its own strong points and downsides, for example:

- Advantages:

  - They are useful for inferring the channel responses in a given PLC network, as long as its topology is known to a certain degree.
  - It is easy to introduce long-term and short-term changes in the channel response.
  - They can provide statistically representative channel responses by using randomly generated topologies.

- Drawbacks:
  - Bottom-up models usually need a lot of information about the PLC channel topology being modeled.
  - Simulation can be way more expensive computationally than in top-down models.

2.1.2 SISO PLC noise characterization

PLC noise is comprised of a number of terms: from perturbations generated by the electrical devices connected to the considered grid to noise coupled to it via radiation or via conduction. According to their waveform, they can be grouped into three main categories: impulsive noise, narrowband interference, and background noise [27]. The number of noise terms may vary considerably among PLC networks and throughout the day.

Impulsive noise is comprised of different components that can also be classified according to:

- Periodic impulsive noise synchronous with the mains. This component appears in a dual manner: as a series of isolated impulses of considerable duration (up to hundreds of microseconds) and amplitude (up to 1.5 V), and as impulse trains in which the number of impulses and separation between them varies from cycle to cycle. Even though these two components show different

characteristics (duration, amplitude, central frequency, bandwidth), both components share some features such as always appearing in the same instant of the mains cycle, having a repetition rate of 50/100 Hz (in Europe), and being usually caused by Silicon Controlled Rectifiers (SCR) in power-supplies.

- Periodic impulsive noise asynchronous with the mains. This noise component takes the form of impulse trains whose constituent impulses have repetition rates that are not related to the mains frequency, ranging from approximately 12 up to 217 kHz. It has been recently shown that these impulse trains always appear at the same instants of the main cycle [77], which allows its categorization as cyclostationary. Nevertheless, there is a great variety of train patterns, sometimes appearing in the vicinity of the zero crossings, around peak mains voltage values, and even during the whole mains cycle.

- Asynchronous impulsive noise. Two types of asynchronous impulsive noise have been observed: isolated impulses with considerable amplitudes and widths, and impulse trains with arbitrary separation between the constituent pulses. This components have an unpredictable nature, with no regular occurrence, and are mostly due to transient states caused by the connection and disconnection of electrical devices.

Narrowband interference is mostly formed by sinusoidal or modulated signals with different origins, e.g., broadcast stations, spurious caused by electrical appliances with a transmitter or a receiver, etc. It usually shows significantly higher level that background noise and, in general, the remaining noise terms. This type of noise can be classified according the following criteria: the shape of its PSD and its satistical properties. According to the shape of their PSD it can be found: interference with multiple discrete frequency components, whose peaks are not harmonically related and are usually located above 4 MHz, and interference with one frequency component, which can be found below 2 MHz and above 20 MHz, e.g., interference from commercial amplitude modulation (AM) radio stations. NB interference can

be classified according to its statistical properties into stationary noise, whose level does not change along the mains cycle, and cyclostationary noise.

Fig. 2.8 depicts the waveform of three measured noise registers. Fig. 2.8 (a) shows a strong periodic impulsive synchronous with the mains component, whereas a noise capture dominated by a cyclostationary narrowband interference (capped with a synchronous periodic impulse) is depicted in Fig. 2.8 (b). Lastly, Fig. 2.8 (c) shows periodic impulsive noise asynchronous with the mains. As seen, they exhibit an almost deterministic behavior which is a key difference between noise in wired scenarios and noise in wireless scenarios.

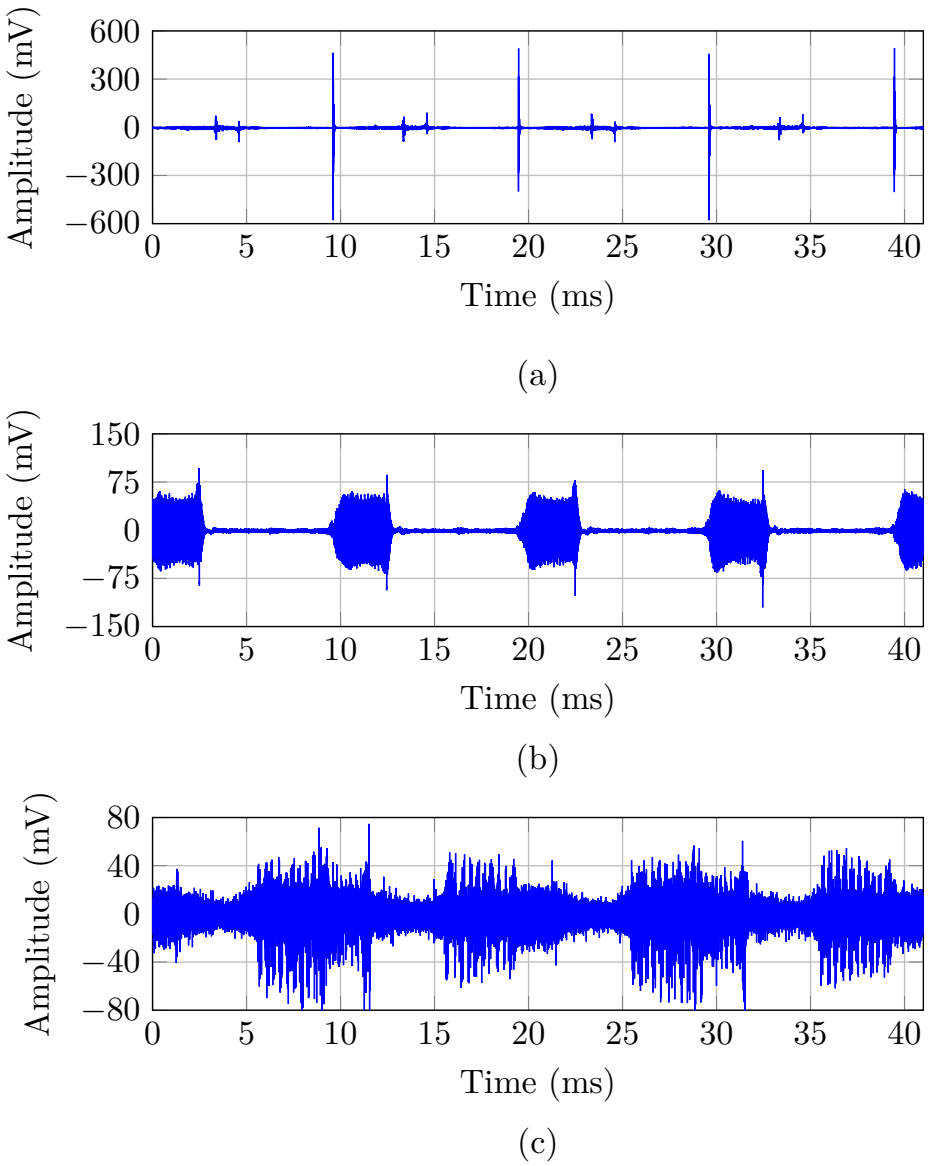

FIGURE 2.8: Illustrative example of three measured indoor PLC noise registers.

As a consequence of the aforementioned terms, the PSD of PLC noise is strongly colored, as illustrated in Fig. 2.9, which depicts the PSD of a measured noise register in the frequency band up to 100 MHz. The zoomed region highlights the periodic peaks corresponding to periodic impulsive noise asynchronous with the mains components. The strong narrowband interference terms above 85 MHz correspond to FM broadcasting emissions.

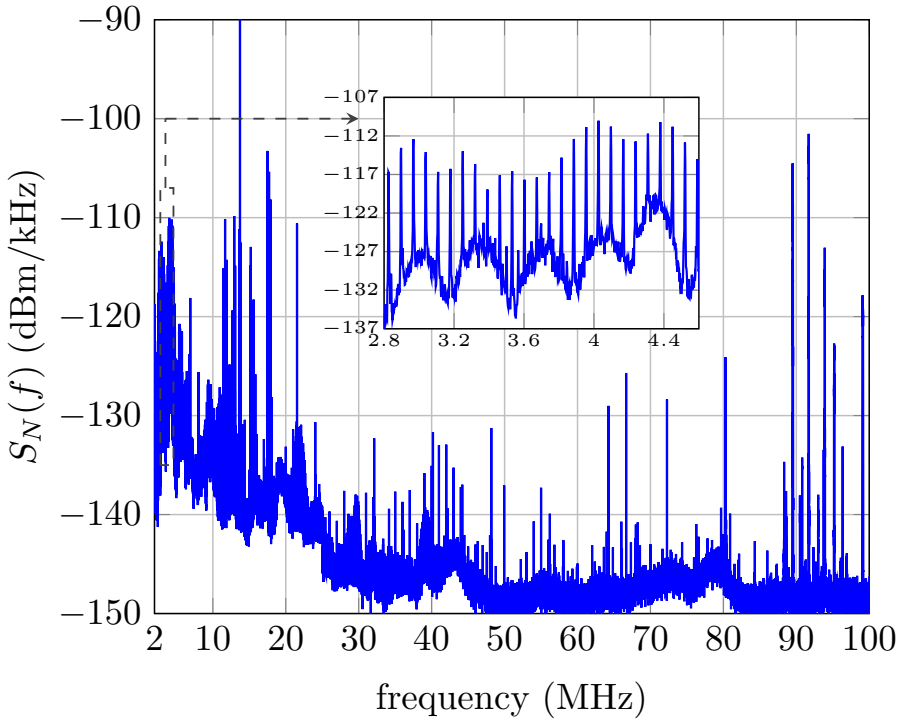

FIGURE 2.9: Representative PSD of a measured indoor PLC noise register.

Background noise comprises the rest of noise types not included in the previous categories. It can be modeled as a colored cyclostationary process, although it can be assumed to be locally stationary for many applications. The PSD of the background noise is much larger at low frequencies than at high ones. This is illustrated in Fig. 2.10, which depicts the PSD of measured noise registers from which the impulsive and narrowband interference terms have been eliminated. Accordingly, the PSD of the background noise can be modelled as [78]

$$S_N(f) = a + bf^c \text{ (dBm/kHz)}, \tag{2.1}$$

with f in MHz.

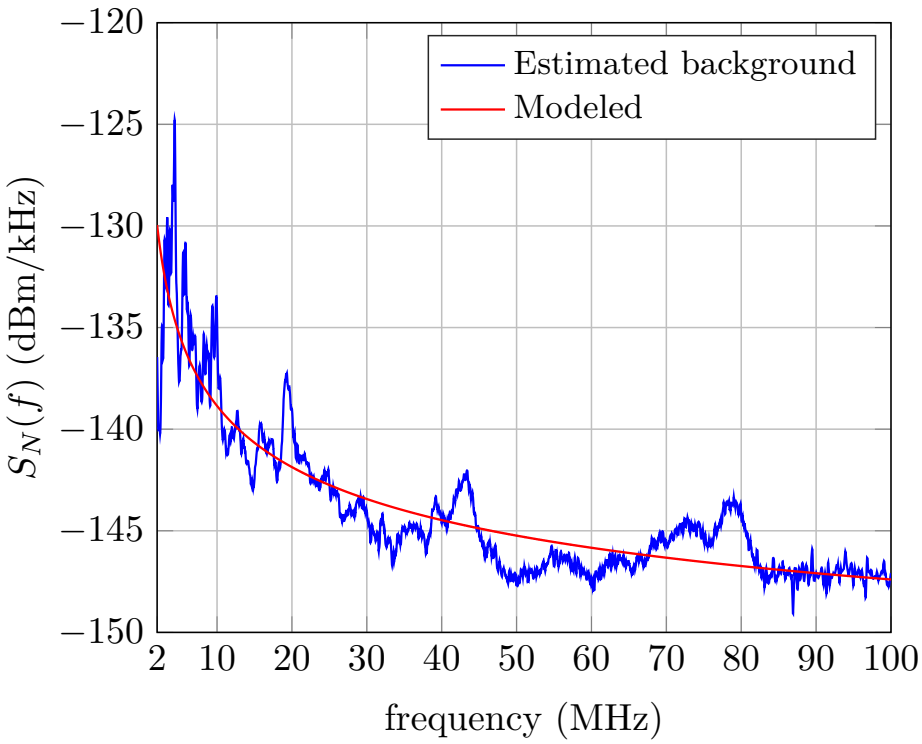

FIGURE 2.10: Estimated PSD of the background noise in Fig. 2.9 and of its best approximation with the model in Eq. (2.1).

Lastly, the amplitude of time-domain PLC noise samples follows a heavy-tailed probability distribution, meaning that extreme values occur much more often than in a Gaussian distribution (due to the impulsive and narrowband interference terms). However, regarding background noise, since it results from the contribution of a large number of independent sources, the Gaussian distribution seems appropriate enough to model the amplitude of this noise component [27].

2.2 MIMO PLC channel response characterization and modelling

This section focuses on the details of MIMO PLC channel characterization and modelling. The first part provides the mathematical relations used to model and evaluate a conventional MIMO system, whereas the second and third subsections provide

a comprehensive overview of state-of-the-art (SotA) MIMO PLC channel response characterization and modelling, respectively.

2.2.1 MIMO multiplexing: mathematical relations

The goal of this section is to summarize the main mathematical relations of MIMO multiplexing systems, emphasizing the role of the *condition number* of the MIMO channel as a metric that is strongly related to the achievable bit rate. Expressions given in this section assume that OFDM is employed and that the carrier bandwidth is narrow enough to assume that each of them undergoes a flat channel with neither inter symbol interference (ISI) nor inter carrier interference (ICI).

MIMO multiplexing exploits the structure of the channel response matrix at each frequency to obtain independent signaling paths that can be used to send multiple data streams in parallel, which increases the data rate. The ratio between the capacities of the MIMO and SISO channels is called multiplexing gain. It can be proved that the maximum gain attainable with an $N \times M$ MIMO system, where N and M denote the number of transmitters and receivers, respectively, is $min\{N, M\}$.

Consider an $N \times M$ MIMO system where the transmitted and received symbol vectors are denoted as $\mathbf{x} = [x_1, x_2, \ldots, x_N]^{\mathrm{T}}$ and $\mathbf{y} = [y_1, y_2, \ldots, y_M]^T$, respectively. Assuming there is neither ISI nor ICI, the MIMO channel output at a given frequency (which is omitted for the sake of clarity) can be expressed as

$$\mathbf{y} = \mathbf{H}\mathbf{x} + \mathbf{u}, \tag{2.2}$$

where $\mathbf{u} = [u_1, u_2, \ldots, u_M]^{\mathrm{T}}$ is the M-dimensional noise vector and

$$\mathbf{H} = \begin{bmatrix} h_{11} & \ldots & h_{1N} \\ \vdots & \ddots & \vdots \\ h_{M1} & \ldots & h_{MN} \end{bmatrix}, \tag{2.3}$$

is the MIMO channel frequency response matrix at the considered carrier frequency, whose rank will be denoted as $R_H = \text{rank}\{\mathbf{H}\}$.

For any MIMO channel matrix $\mathbf{H}$ we can obtain its singular value decomposition (SVD) as

$$\mathbf{H} = \mathbf{U}\mathbf{\Sigma}\mathbf{V}^{\mathrm{H}}, \tag{2.4}$$

where $(\cdot)^{\mathrm{H}}$ denotes the Hermitian operator, the $M \times M$ matrix $\mathbf{U}$ and the $N \times N$ matrix $\mathbf{V}$ are unitary matrices and $\mathbf{\Sigma}$ is an $M \times N$ diagonal matrix with R_H non-zero singular values σ_i. These singular values have the property that $\sigma_i = \sqrt{\lambda_i}$ for λ_i the i-th largest eigenvalue of $\mathbf{H}\mathbf{H}^{\mathrm{H}}$.

The parallel decomposition of the channel is obtained by defining a transformation on the channel input $\mathbf{x}$ and output $\mathbf{y}$ via transmit precoding and receiver shaping as follows

$$\mathbf{x} = \mathbf{V}\mathbf{s}, \tag{2.5}$$

$$\mathbf{z} = \mathbf{U}^{\mathrm{H}}\mathbf{y}, \tag{2.6}$$

where $\mathbf{s}$ is the input vector comprising the original symbols and $\mathbf{z}$ is the resulting output vector after receiver shaping.

This transmit precoding and receiver shaping transform the MIMO channel into R_H parallel SISO channels with input $\mathbf{s}$ and output $\mathbf{z}$ since

$$\begin{aligned}\mathbf{z} = \mathbf{U}^{\mathrm{H}}(\mathbf{H}\mathbf{x} + \mathbf{u}) = \mathbf{U}^{\mathrm{H}}(\mathbf{U}\mathbf{\Sigma}\mathbf{V}^{\mathrm{H}}\mathbf{x} + \mathbf{u}) = \mathbf{U}^{\mathrm{H}}(\mathbf{U}\mathbf{\Sigma}\mathbf{V}^{\mathrm{H}}\mathbf{V}\mathbf{s} + \mathbf{u}) = \\ \mathbf{U}^{\mathrm{H}}\mathbf{U}\mathbf{\Sigma}\mathbf{V}^{\mathrm{H}}\mathbf{V}\mathbf{s} + \mathbf{U}^{\mathrm{H}}\mathbf{u} = \mathbf{\Sigma}\mathbf{s} + \mathbf{n},\end{aligned} \tag{2.7}$$

where $\mathbf{n} = \mathbf{U}^{\mathrm{H}}\mathbf{u}$ and $\mathbf{\Sigma}$ is the diagonal matrix of singular values of $\mathbf{H}$ with σ_i on the i-th diagonal position and zeros everywhere else. Assuming that the channel noise $\mathbf{u}$ is uncorrelated between ports and with equal power, so is $\mathbf{n}$ because $\mathbf{U}$ is a unitary matrix. Furthermore, if $\mathbf{u}$ is Gaussianly distributed, $\mathbf{n}$ is Gaussianly distributed as well.

The MIMO decomposition shown in Eq. (2.7) allows a simple proxy for the MIMO channel capacity for a fixed[2] channel matrix $\mathbf{H}$ known at transmitter and receiver side. The achievable bit rate can be approximated by the sum of the achieved bit rates on each of the independent parallel channels when the transmit power is optimally allocated between these channels, which is usually attained by applying the water-pouring strategy.

Under the aforementioned assumption for the noise and applying the well-known Shannon-Hartley theorem to the independent parallel channels, the achieved bit rate, R, by a given carrier can be written as

$$R = \max_{P_i:\sum_{i=1}^{R_H} P_i \leq P} \left\{ \sum_{i=1}^{R_H} B \log_2(1 + \frac{\lambda_i P_i}{\beta \sigma^2}) \right\}, \tag{2.8}$$

where B is the channel bandwidth, P the total available power at the transmitter side, P_i the power allocated to the i-th channel, σ^2 the noise power, and β is the so-called signal-to-noise ratio (SNR) gap to capacity, which accounts for the SNR penalty due to the use of a practical encoder. For uncoded square QAM constellations, $\beta = \frac{1}{3}\left[Q^{-1}\left(SER/4\right)\right]^2$, where SER is the symbol error probability [79].

This expression indicates that, at high SNR, the achievable bit rate increases linearly with the number of degrees of freedom in the channel. On the other hand, when $\lambda_1 \gg \lambda_i \ \forall i \in [2, R_H]$, the multiplexing gain is low. Hence, the condition number of the channel matrix, which is the ratio of the largest to the lowest singular value,

$$\kappa \text{ (dB)} = 20 \log_{10}\left(\frac{\sigma_1}{\sigma_{R_H}}\right) = 10 \log_{10}\left(\frac{\lambda_1}{\lambda_{R_H}}\right), \tag{2.9}$$

is inversely related to the multiplexing gain: the larger the value of κ, the lower the multiplexing gain. When the channel matrix has $R_H = 1$, all MIMO streams are perfectly correlated and $\kappa \to \infty$. By contrast, when all singular values are equal, $\kappa = 0$ dB. Hence, the condition number measures of the correlation of the MIMO

[2]Note that, as stated in 2.1.1, changes in indoor PLC channels usually take longer than the conventional OFDM symbol duration. Therefore the LTI approximation can be adopted.

paths, which is referred to as spatial correlation: the larger the value of κ, the larger the spatial correlation.

To account for the limited number of bits per symbol of the employed constellations, which is actually limited to 12 bits, Eq. (2.8) can be reformulated as

$$R = \max_{P_i:\sum_{i=1}^{R_H} P_i \leq P} \left\{ \sum_{i=1}^{R_H} B \min(12, \log_2(1 + \frac{\lambda_i P_i}{\beta \sigma^2})) \right\}. \tag{2.10}$$

The correlation of the noise in different MIMO ports can be exploited to increase the presented data rates by means of a whitening transformation applied at the receiver side. The latter transforms the system into a white noise (between ports) with equal power, as considered in (2.10). To this end, let us assume that the noise autocorrelation matrix is given by $\mathbf{\Gamma_u} = \mathbb{E}\{\mathbf{u}\mathbf{u}^{\mathrm{H}}\}$, since it is an Hermitian matrix, the following decomposition can be applied

$$\mathbf{\Gamma_u} = \mathbf{E}\mathbf{\Delta}\mathbf{E}^{\mathrm{H}}, \tag{2.11}$$

where $\mathbf{\Delta}$ is a diagonal matrix with real and positive diagonal values and $\mathbf{E}$ is a unitary matrix. Therefore, by applying the following transformation $\mathbf{\Delta}^{\frac{-1}{2}}\mathbf{E}^{\mathrm{H}}$ to the received signal (before the receiver shaping $\mathbf{U}^{\mathrm{H}}$ shown above) noise can be whitened and normalized since the autocorrelation matrix of $\mathbf{u_1} = \mathbf{\Delta}^{\frac{-1}{2}}\mathbf{E}^{\mathrm{H}}\mathbf{u}$ is given by

$$\begin{aligned} \mathbf{\Gamma_{u_1}} = \mathbb{E}\{\mathbf{u_1}\mathbf{u_1}^{\mathrm{H}}\} = \mathbb{E}\{\mathbf{\Delta}^{\frac{-1}{2}}\mathbf{E}^{\mathrm{H}}\mathbf{u}\mathbf{u}^{\mathrm{H}}\mathbf{E}\mathbf{\Delta}^{\frac{-1}{2}}\} = \mathbf{\Delta}^{\frac{-1}{2}}\mathbf{E}^{\mathrm{H}}\mathbb{E}\{\mathbf{u}\mathbf{u}^{\mathrm{H}}\}\mathbf{E}\mathbf{\Delta}^{\frac{-1}{2}} = \\ \mathbf{\Delta}^{\frac{-1}{2}}\mathbf{E}^{\mathrm{H}}\mathbf{E}\mathbf{\Delta}\mathbf{E}^{\mathrm{H}}\mathbf{E}\mathbf{\Delta}^{\frac{-1}{2}} = \mathbf{I}_M, \end{aligned} \tag{2.12}$$

where $\mathbf{I}_M$ is the $M \times M$ identity matrix.

So, by applying the noise whitening transformation above and then applying transmit precoding and receiver shaping over the resulting new channel, $\tilde{\mathbf{H}} = \mathbf{\Delta}^{\frac{-1}{2}}\mathbf{E}^{\mathrm{H}}\mathbf{H}$, it can be obtained a system with $R_{\tilde{H}}$ independent channels, with gain $\tilde{\sigma}_i = \sqrt{\tilde{\lambda}_i}$ each, and uncorrelated unitary-power noise.

2.2.2 MIMO PLC channel response characterization

A MIMO channel can be regarded as a collection of SISO channels. Since PLC SISO channels were already discussed in section 2.1.1, in this section we will be focusing on the relation between the SISO channel responses that comprise the complete MIMO channel response. The relation between SISO channel responses is usually called *spatial correlation* and quantified by means of the condition number given in Eq. (2.9).

In a wireless media, channel responses are usually uncorrelated when transmitters and receivers are located far away from each other. This is not the case in indoor MIMO PLC channel responses where, not only the existing transmitting/receiving ports are close to each other, but the wiring that is being traversed by the signal is usually bundled tightly so crosstalk phenomena is strong, which increases channel response correlation.

The work in [46] analyses the MIMO-PLC channels based on measurements obtained during the ETSI STF410 field measurement campaign in six European countries. STF410 recorded (among many other measurements) the transfer functions of all individual MIMO paths in frequencies up to 100 MHz. The channel analysis in this paper compares different MIMO configurations and investigates the attenuation, correlation and capacity of the MIMO-PLC channel response. Specifically, it was shown that the MIMO PLC channel response has a rather high spatial correlation as shown in Figure 2.11. Moreover, that work includes an analysis where, by exploiting feeding options, a 2×4 MIMO channel can be used to achieve double the capacity of its SISO counterpart.

Figure 2.11 shows that for 20% of the channels (cumulative probability of 0.8) the smallest singular value is at least 10 times smaller than the largest singular value. In [47] a similar channel correlation profile captured from measurements is shown.

Regarding the relation between channel spatial correlation and frequency, [47] shows that the average value of the correlation is almost constant with respect to

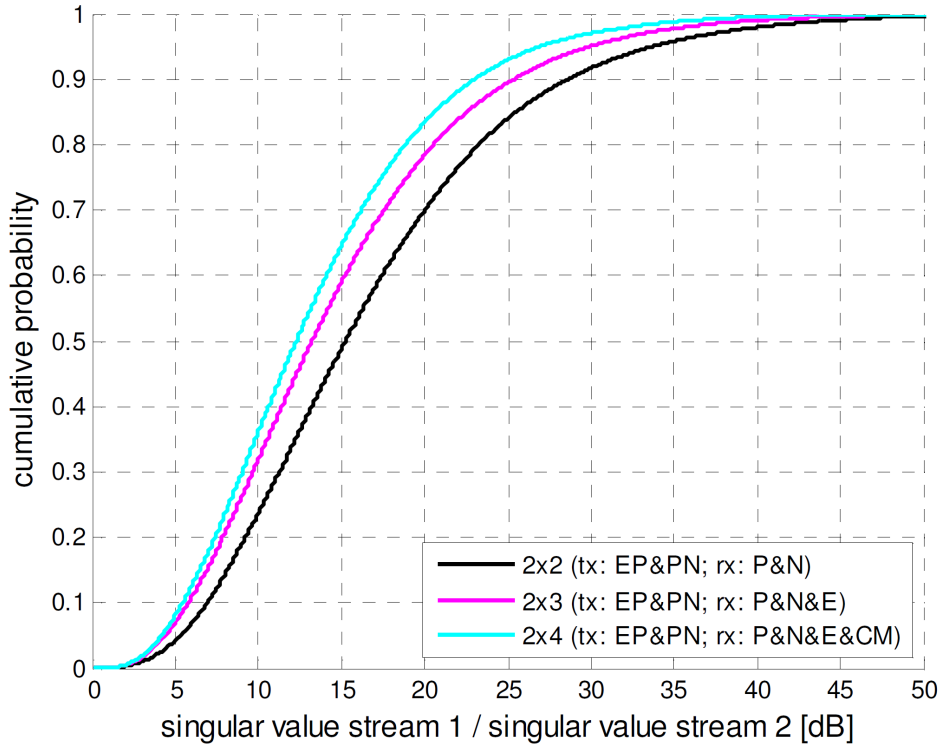

FIGURE 2.11: Spatial Correlation illustrated via the cumulative probability of the ratio of the singular values obtained from a measurement campaign in six European countries, [46] Fig. 11.

the frequency.

Lastly, the influence that channel topology and coupling strategies have on MIMO powerline channel characteristics is studied in [80] where it highlights that there is a strong dependence between these features.

2.2.3 MIMO PLC channel response modelling

Since SISO PLC channel response modelling strategies were covered in section 2.1.1, this section will be focused on those channel response models which feature MIMO capabilities. However, in contrast to the SISO, the number of available MIMO channel model proposals is quite limited.

Top-down models

Similarly to the SISO case, top-down MIMO models usually employ one of the two following strategies: echo-based models and (multidimensional) RVs.

The extension of the echo-based model to MIMO channels was proposed in [70]. It firstly generates a SISO channel response from which the remaining responses of the MIMO channel are obtained by using spatial correlation matrices derived from measurements.

Regarding the RV modeling approach, the extension to MIMO is based on the generation of as many channel (frequency) response vectors as existing MIMO paths, e.g., in a 2×3 MIMO channel the number of paths is 6. This task requires knowledge of correlation between elements of a same vector (frequency correlation) and correlation between elements from different vector (spatial correlation). This strategy is applied in [68].

Bottom-up models

The need to accommodate for a third conductor to model MIMO PLC channel topologies entails that the conventional two-conductor transmission line approach is no longer valid and an approach based on MTL is needed. Appendix A provides a summary of the analytical expressions that relate voltages and currents in MTL-based networks.

The most relevant work regarding the use of MTL for MIMO indoor broadband PLC channel modelling was proposed in [51]. It showed that when different cross sections are used to model the deployed wiring, the resultant channel responses would vary as well in both the direct and crosstalk channels. However, the implementation proposed in that work produced artificially-high symmetric paths which yielded MIMO channel responses with unrealistic spatial correlation for two reasons: the spatial correlation presents always the same value across frequencies and channels, and it is notably lower than the spatial correlation measured from real scenarios.

2.3 MIMO PLC noise characterization

Noise correlation is usually analyzed in the time domain, e.g., the "white" behavior in the well-known AWGN approximation makes reference to the uncorrelated nature of noise between consecutive time samples. However, in a MIMO system, noise correlation has an added dimension worthy of analysis: spatial correlation. Similarly to what was previously discussed in Section 2.2, noise spatial correlation makes reference to the correlation between noise captured in different ports.

MIMO PLC noise correlation is analyzed in [49] in the frequency band up to 88 MHz. It shows that spatial correlation is higher at low frequencies (under 30 MHz), as shown in Fig. 2.12, where the averaged noise correlation coefficient in the frequency range 2-88 MHz is displayed and the averaging is performed over a set of 100 measured noise registers. It is worth noting that this work conducted the analysis on the frequency domain and the measurements employed were obtained by HomePlug AV2-compliant receivers, therefore they are biased by their technical specification settings, e.g., the frequency range is limited to the 2-88 MHz range, the discrete Fourier transform (DFT) size, and non-adjacent DFT windows because of the cyclic prefix.

Moreover, the channel performance gain from exploiting noise correlation was also studied in [49] and it stated that, in poor channels, such performance gain could be as high as 40%. Note that the performance of MIMO systems operating under correlated noise conditions, can be improved by applying noise whitening transformations which take advantage of this noise profile, as already shown in subsection 2.2.1. In short, noise whitening transformations can be seen as the removal from a port of all noise information that it shares with other ports, hence the term *whitening* making reference to them producing *spatially* uncorrelated noise components. If noise is highly correlated, a high amount of information is shared between ports, therefore the removal of all this information from a port would yield a new port with a much weaker noise component, which would improve the port SNR and by

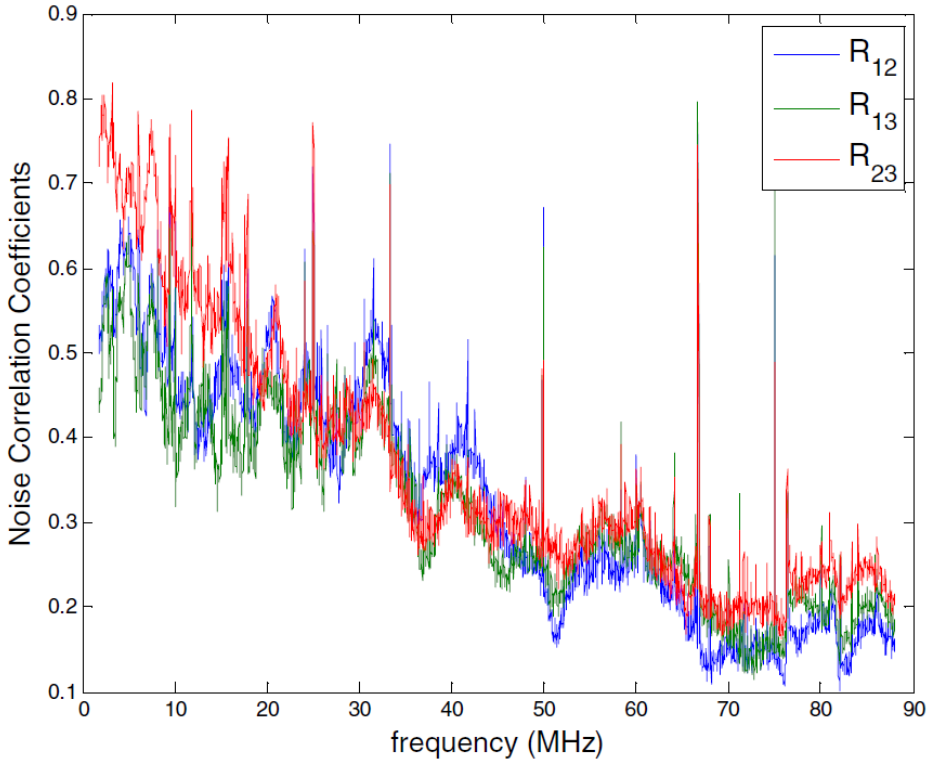

FIGURE 2.12: Average noise correlation coefficient obtained from 100 measured noise registers. Extracted from Fig. 5 in [49].

extension the performance of the MIMO system.

Lastly, it is worth noting that the narrowband interference component of MIMO PLC noise[3] may exhibit very high power and highly correlated profiles at certain frequencies. This is due to receivers located very close to each other while the source of the interference is transmitting from far away a high power signal which is captured simultaneously on all ports, thus the high spatial correlation of this noise component. Therefore a system operating in a MIMO channel dominated by strong narrowband interference, could theoretically take advantage of the correlated nature of noise to greatly enhance its performance by applying noise whitening transformations.

[3]As a reminder, please note that in subsection 2.1.2 it is stated that noise components are usually categorized into three main groups: impulsive noise, narrowband interference and background noise.

Chapter 3

Publications

3.1 An MTL-Based Channel Model for Indoor Broadband MIMO Power Line Communications

- **DOI**. 10.1109/JSAC.2016.2566178
- **Reference**. [41]
- **Abstract**. The recent release of indoor power line communication (PLC) standards with multiple-input multiple-output (MIMO) capabilities has led to the need for channel models that reflect the multiconductor nature of the grid. This paper proposes a model, based on the multiconductor transmission line theory, along with a random PLC channel generator operating in the frequency range from 1 to 100 MHz. Its distinctive features are the modeling of three key elements: the asymmetry in the layout caused by the derivations to the light switches, the impedance of the devices connected to the three wires of the grid, and the variable distance between the conductors in loose wiring deployments. The influence of these elements in the spatial correlation between the streams of the MIMO links is studied and compared with measurements.

3.2 Analysis of the Spatial Correlation of Indoor MIMO PLC Channels

- **DOI**. 10.1109/LCOMM.2016.2616341
- **Reference**. [42]
- **Abstract**. In this letter, an analysis of the spatial correlation of multiple-input multiple-output (MIMO) power line communications (PLC) channels in the frequency range 1–80 MHz is provided, where the term spatial correlation refers to the relation between the paths that form the MIMO channel matrix. The study is based on a large set of 2×2 MIMO channels measured in four different countries. The presented statistical analysis of the condition number reveals three important facts. First, the spatial correlation is almost independent of frequency, which has important implications in the development of top-down MIMO PLC channel models. Second, the use of an alternative injection method can notably reduce the spatial correlation and, consequently, increase the system bit-rate. Third, there exist countries whose channels have larger spatial correlation values than others. Since spatial correlation plays a key role in the performance of MIMO PLC systems, a hypothesis relating the type of wiring deployed in the indoor power grid to the spatial correlation is given and supported by simulations.

3.3 Analysis and Exploitation of the Noise Correlation in MIMO Power Line Communications in the FM Band

- **DOI**. 10.1109/LCOMM.2017.2787714
- **Reference**. [43]
- **Abstract**. This letter analyzes noise correlation in multiple-input multiple-output (MIMO) power line communications (PLC) in the 2–108 MHz band. The focus is on the 88–108 MHz range, which in most countries is assigned to frequency modulation (FM) broadcasting. The study reveals that noise correlation is very high in frequencies impaired by FM ingress and very low in frequencies where background noise dominates, yielding a bimodal behavior. The influence of noise correlation in orthogonal frequency division multiplexing systems is also addressed. It is shown that the spectral leakage of the rectangular window spills the correlation introduced by FM signals to the adjacent frequencies. Hence, the lower the number of carriers, the larger the performance gain obtained by adding a whitening transformation to linear precoded systems. Based on these findings, the feasibility of MIMO PLC in the FM band is assessed. Results indicate that 50% of the channels attain bitrates larger than 9 Mbit/s with an injected power spectral density as low as -100 dBm/Hz.

Chapter 4

Conclusions

In this final chapter, the main achievements which arise from the contributions of this work are outlined. Besides, some future lines regarding the work developed in this dissertation are suggested.

4.1 Achievements

This thesis has focused on the study of indoor broadband MIMO PLC channels. It has addressed the following key aspects concerned with them: analysis of the spatial correlation of the channel response and the noise and channel response modeling. The main contributions achieved in this context can be summarized as follows:

- **MIMO PLC channel response characterization**. The influence of several aspects on the spatial correlation of the channel response has been assessed. Firstly, it has been shown by means of measurements that spatial correlation in PLC channels does not show a significant dependence with respect to frequency. This result is important for the development of realistic top-down MIMO PLC channel models. In second place, it has been shown that different injection strategies yield different spatially correlated MIMO channel responses, e.g., when the typical differential injection is used, the resultant channel response presents higher spatial correlation than the case where pseudo-differential injection is used. This is a valuable take since a MIMO channel

response with low correlation usually yields better performance. Lastly, it has been pointed out that spatial correlation is strongly dependent on type of wiring used in the underlying power network, which we then confirmed by means of simulations using a bottom-up MIMO PLC channel model under different wiring configurations.

- **MIMO PLC channel response modeling**. Existing bottom-up channel response models based on MTL theory did not capture spatial correlation in a realistic way. The hypothesis was that, for spatial correlation to manifest in a realistic manner, some degree of asymmetry between the SISO paths that comprise channel was needed. These asymmetries were captured in our proposed MIMO PLC bottom-up channel response model via the addition of the following features: variable separation between conductors, non-symmetric loads between ports and asymmetric network layout (parts of the grid where only one wire is present), e.g., the lighting circuit that connect a switch with the rest of the network.

  A MIMO PLC channel response simulator was built using the model above and a random topology generator which allows the systematic creation of realistic indoor PLC networks. Channel responses obtained using this simulator were compared against a set of measured channel responses, obtaining very good fits on both, spatial correlation (MIMO) and frequency response (SISO).

- **Characterization and exploitation of MIMO PLC noise**. There are studies that analyze the spatial correlation of noise in MIMO PLC channels, however they do not review the distribution of noise spatial correlation in different bands. The analysis of this noise distribution is relevant since noise may show special correlation profiles in some bands, e.g., the 88-100 MHz band, which in most countries is assigned to FM broadcasting services. In this work, an estimate of the probability density function (PDF) of the spatial correlation of the noise in 20 MHz-wide bands has been obtained from measurements.

Results indicate that correlation is very high in the FM band, where signals transmitted from a distant source are almost equally coupled to the three conductors of the power network. The exploitation of this correlation by means of a whitening transformation has been assessed, showing that PLC could be feasible in the FM band by applying linear precoding and whitening transformations, even with an injected PSDs as low as -100 dBm/Hz. The influence of the spectral leakage caused by the DFT, which spreads the FM interference to nearby frequencies, has been also evaluated.

4.2 Suggestions for further work

This dissertation can be used as the starting point for a number of issues that need further study. Some examples are indicated below.

- **Channel response models**. Even though the channel response model proposed is based on the bottom-up strategy, top-down models are still interesting due to their computational efficiency and flexibility. There are numerous top-down PLC channel models available, although we observed that most of them offered quite an unrealistic spatial correlation profile. For example, the top-down MIMO model proposed in [68] shows unrealistic narrow dispersion on coherence bandwidth and DS, whilst [69] improves these features but only proposes a SISO model. We believe that there is still room for improvement in this field whose results could be used to develop better tuned strategies for these channels.

- **Characterization and exploitation of determinism in MIMO PLC noise.** Some recent works focused on NB like [81] show that noise in MIMO scenarios is quasi deterministic, i.e., noise captured in a port is a delayed and scaled version of noise on other port. We believe it would be worth studying

this phenomena in a BB environment and develop strategies that exploit this feature.

Appendix A

Summary of MTL relations

This appendix summarizes the analytical expressions that relate the voltages and currents in the MTL-based networks used in [41]. To this end, the characterization of networks with multiple ports by means of transmission matrices is firstly presented. Then, the elements of the transmission matrix of an MTL are expressed in terms of its per-unit-length (PUL). To this end, the following notation is employed. Scalar variables are written using italic letters. Matrices and column vectors are written in boldface, the former in capital letters. The transpose operator is denoted as $(\cdot)^{\mathrm{T}}$. The imaginary unit is written as $j = \sqrt{-1}$. $\mathbf{I}_n$ is the $n \times n$ identity matrix, while $\mathbf{0}_n$ is an $n \times n$ zero matrix. Given the $m \times n$ matrix $\mathbf{A}$,

$\mathbf{A}(i, j)$ denotes the element of $\mathbf{A}$ located in the i-th row and j-th column,

$\mathbf{A}(i, :)$ denotes the i-th row-vector of $\mathbf{A}$,

$\mathbf{A}(:, j)$ denotes the j-th column-vector of $\mathbf{A}$.

A.1 Matrix characterization of $2n$-port networks and n-port loads

A.1.1 Transmission matrix

Given a network with n input and n output ports, like network A in Fig. A.1, its steady-state voltage and current phasors at frequency f can be related by means of

the $2n \times 2n$ transmission matrix $\mathbf{T}$ as[1]

$$\left[V_1^{\text{out}}, \ldots, V_n^{\text{out}}, I_1^{\text{out}}, \ldots, I_n^{\text{out}}\right]^{\text{T}} = \mathbf{T}\left[V_1^{\text{in}}, \ldots, V_n^{\text{in}}, I_1^{\text{in}}, \ldots, I_n^{\text{in}}\right]^{\text{T}} \tag{A.1}$$

where $I_0^{in} = \sum_{i=1}^{n} I_i^{in}$ and $I_0^{out} = \sum_{i=1}^{n} I_i^{out}$, and $V_i^{\text{in/out}}$ is the voltage between terminal i and terminal 0 at the input/output side of the network. The terminal 0 is also called "reference terminal" and it is usually represented on the figures as the bottom-most terminal.

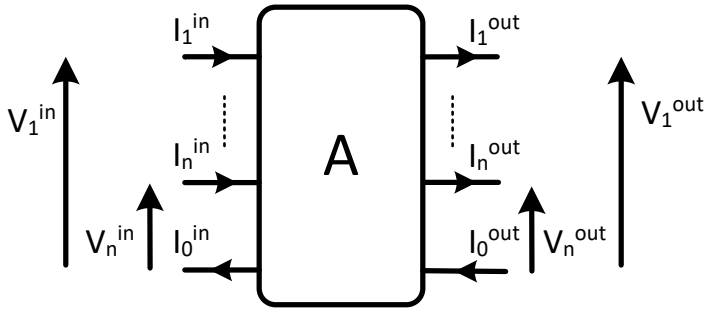

FIGURE A.1: Voltages and currents in a $2n$-port network.

The transmission matrix $\mathbf{T}$ can be conveniently written as a block matrix,

$$\mathbf{T} = \begin{bmatrix} \mathbf{T}_{11} & \mathbf{T}_{12} \\ \mathbf{T}_{21} & \mathbf{T}_{22} \end{bmatrix} \tag{A.2}$$

where $\mathbf{T}_{ij}$ are $n \times n$ matrices.

A.1.2 Input impedance matrix

Definition of the input impedance matrix

Given a generic n-port load, like load *B* in Fig. A.2, its voltages and currents phasors at a given frequency can be related by means of the $n \times n$ input impedance matrix $\mathbf{Z}^{\text{in}}$ as

$$\left[V_1^{\text{in}}, \ldots, V_n^{\text{in}}\right]^{\text{T}} = \mathbf{Z}^{\text{in}}\left[I_1^{\text{in}}, \ldots, I_n^{\text{in}}\right]^{\text{T}} \tag{A.3}$$

[1]Note that the transmission matrix $\mathbf{T}$ is actually $\mathbf{T}(f)$ but, for convenience, we'll omit the frequency notation.

where $I_0^{in} = \sum_{i=1}^{n} I_i^{in}$.

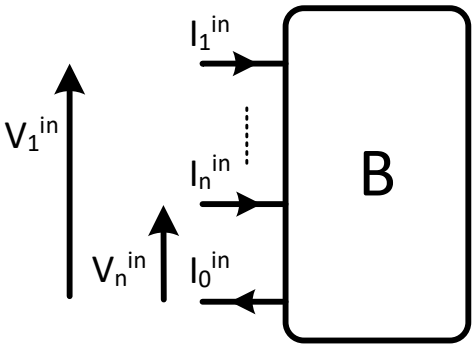

FIGURE A.2: Voltage and current in an n-port load.

Input impedance matrix of delta-style loads

Given the delta-style load depicted in Fig. A.3, its input impedance matrix $\mathbf{Z}^{\text{in}}$ is given by

$$\mathbf{Z}^{\text{in}} = \mathbf{Y}_{\text{in}}^{-1} \tag{A.4}$$

$$\mathbf{Y}^{\text{in}} = \begin{bmatrix} y_{11} + y_{12} & -y_{12} \\ -y_{12} & y_{22} + y_{12} \end{bmatrix} \tag{A.5}$$

where $y_{ij} = z_{ij}^{-1}$ and z_{ij} is the impedance value of its correspondent load in Fig. A.3.

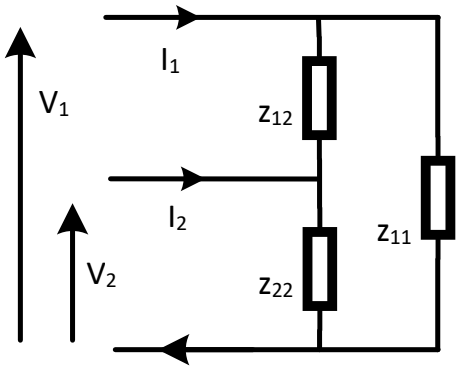

FIGURE A.3: Circuit model of the delta-style loads used in [41].

Input impedance matrix of loaded $2n$-port network

Let us consider the structure depicted in Fig. A.4, where the voltage and current phasors of the $2n$-port network are related by means of the transmission matrix $\mathbf{T}$ as,

$$[V_1^A,\ldots,V_n^A,I_1^A,\ldots,I_n^A]^{\mathrm{T}}=\underbrace{\begin{bmatrix}\mathbf{T}_{11} & \mathbf{T}_{12}\\ \mathbf{T}_{21} & \mathbf{T}_{22}\end{bmatrix}}_{\mathbf{T}}[V_1^B,\ldots,V_n^B,I_1^B,\ldots,I_n^B]^{\mathrm{T}}, \tag{A.6}$$

and the ones of the n-port load by the input impedance matrix $\mathbf{Z}_{\mathrm{B}}^{\mathrm{in}}$ as $[V_1^B,\ldots,V_n^B]^{\mathrm{T}}=\mathbf{Z}_{\mathrm{B}}^{\mathrm{in}}[I_1^B,\ldots,I_n^B]^{\mathrm{T}}$.

The input voltage and current phasors can then be expressed as $[V_1^A,\ldots,V_n^A]^{\mathrm{T}}=\mathbf{Z}_{\mathrm{A}}^{\mathrm{in}}[I_1^A,\ldots,I_n^A]^{\mathrm{T}}$, where the impedance matrix of the whole system, $\mathbf{Z}_{\mathrm{A}}^{\mathrm{in}}$, is given by

$$\mathbf{Z}_{\mathrm{A}}^{\mathrm{in}}=(\mathbf{T}_{11}-\mathbf{Z}_{\mathrm{B}}^{\mathrm{in}}\mathbf{T}_{21})^{-1}(\mathbf{Z}_{\mathrm{B}}^{\mathrm{in}}\mathbf{T}_{22}-\mathbf{T}_{12}). \tag{A.7}$$

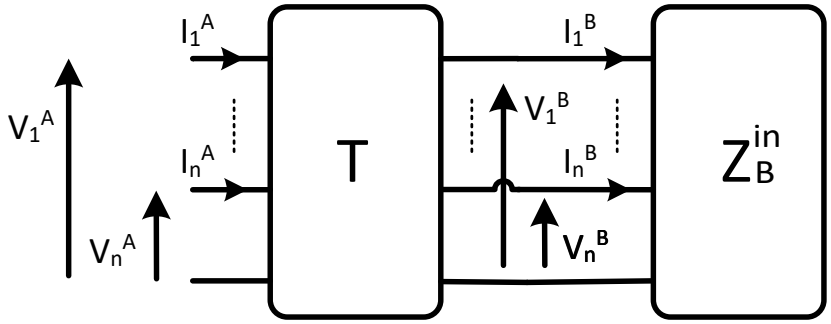

FIGURE A.4: A $2n$-port network with transmission matrix $\mathbf{T}$ ended in an n-port load with input impedance matrix $\mathbf{Z}^{\mathbf{in}}$.

A.1.3 Transmission matrix of a parallel load

The $2n\times 2n$ transmission matrix $\mathbf{T}$ of a $2n$-port network consisting of $(n+1)$ ideal conductors with an n-port load with impedance matrix $\mathbf{Z}^{\mathrm{in}}$ attached in parallel, as

shown in Fig. A.5, is given by

$$\begin{aligned} \mathbf{T}_{11} &= \mathbf{T}_{22} = \mathbf{I}_n, \\ \mathbf{T}_{12} &= \mathbf{0}_n, \\ \mathbf{T}_{21} &= -\mathbf{Z}_{\text{in}}^{-1} \end{aligned} \tag{A.8}$$

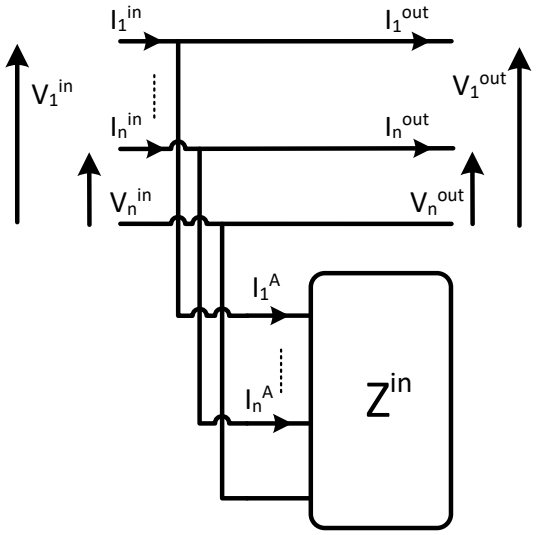

FIGURE A.5: Network consisting of $(n+1)$ ideal conductors with an n-port load attached in parallel.

A.1.4 Equivalent 2-port network of an $2n$-port network

Given a $2n$-port network with $2n \times 2n$ transmission matrix $\mathbf{T}$, if all currents but the i-th input and the j-th output ones are set to zero,

$$\begin{aligned} I_x^{\text{in}} &= 0 \; \forall x \neq i, \\ I_y^{\text{out}} &= 0 \; \forall y \neq j, \end{aligned}$$

then an equivalent 2-port network as the one shown in Fig. A.6 and Fig. A.7 is obtained. Its 2×2 transmission matrix $\mathbf{T}^{\text{eq}}$ can be expressed as

$$\mathbf{T}^{\text{eq}} = \begin{bmatrix} t_{11}^{\text{eq}} & t_{12}^{\text{eq}} \\ t_{21}^{\text{eq}} & t_{22}^{\text{eq}} \end{bmatrix},$$

with

$$t_{11}^{\text{eq}} = -\mathbf{\Gamma}^{-1}(j,:)\mathbf{T}(:,i),$$
$$t_{12}^{\text{eq}} = -\mathbf{\Gamma}^{-1}(j,:)\mathbf{T}(:,n+i),$$
$$t_{21}^{\text{eq}} = -\mathbf{\Gamma}^{-1}(n+1,:)\mathbf{T}(:,i),$$
$$t_{22}^{\text{eq}} = -\mathbf{\Gamma}^{-1}(n+1,:)\mathbf{T}(:,n+i),$$

where the $2n \times 2n$ matrix $\mathbf{\Gamma}$ is given by

$$\mathbf{\Gamma}(1:n, 1:n) = -\mathbf{I}_n,$$
$$\mathbf{\Gamma}(n+1:2n, 1:n) = \mathbf{0}_n,$$
$$\mathbf{\Gamma}(:, n+2:2n) = \mathbf{T}(:, [1, \ldots, i-1, i+1, \ldots, n]),$$
$$\mathbf{\Gamma}(p, n+1) = 0,\ p \in [1, 2, .., n+j-1, n+j+1, ..., 2n],$$
$$\mathbf{\Gamma}(n+j, n+1) = -1.$$

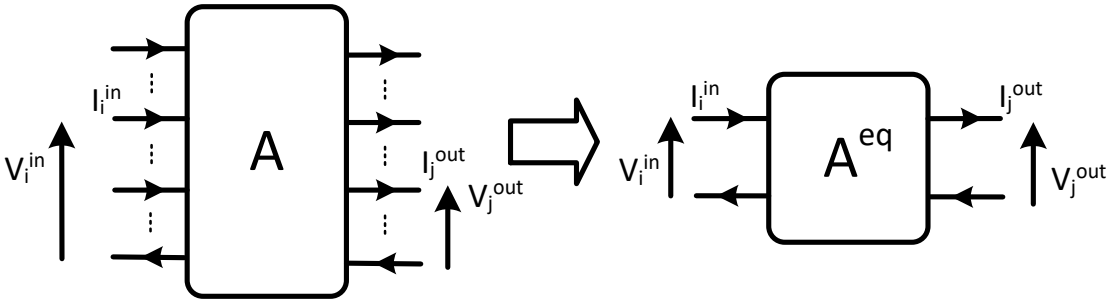

FIGURE A.6: An illustration of the equivalent 2-port network of a $2n$-port network. The i-th and j-th conductors are the only ones with non-zero input and output currents respectively.

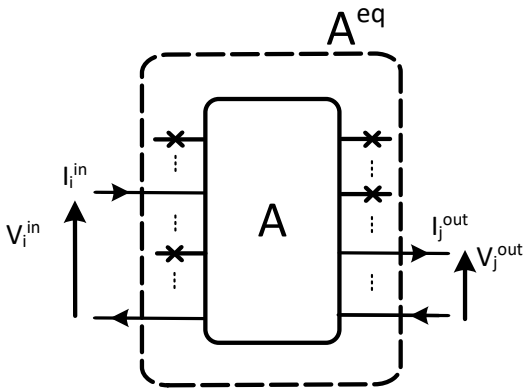

FIGURE A.7: An illustration of the equivalent 2-port network of the $2n$-port network depicted in Fig. A.6. The i-th and j-th conductors are the only ones with non-zero input and output currents respectively.

A.1.5 Voltage response of a 2-port network

The voltage response $H = V^{\text{out}}/V^{\text{in}}$ of a 2-port network[2], like the one depicted in Fig. A.8, with 2×2 transmission matrix **T**, is given by

$$H = t_{11} - \frac{t_{12}t_{21}}{t_{22}} \tag{A.9}$$

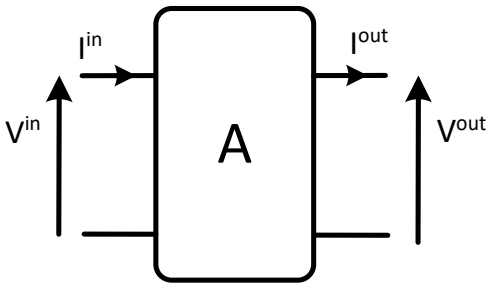

FIGURE A.8: Representation of a 2-port network.

[2]Note that a 2-port network is a special case of the $2n$-port network where $n = 1$. This case has been included for completeness.

A.2 Characterizaton of an MTL by means of transmission matrices

In this section, a brief review of the relations used to characterize an $(n+1)$-conductor MTL as a $2n$-port network using transmission matrices is provided. Presented relations have been taken from [82] and are given here to ease the understanding of the expressions used in our models in [41].

A.2.1 The PUL model of an MTL

Transmission line theory is needed when lines are electrically long enough so that the wave nature of the transmission must be taken into account. MTL are structures that can guide electromagnetic waves in a contained manner in a frequency range from zero up to where the wavelength becomes comparable to the cross-sectional dimension of the structure. Under some assumptions (given at the end of this section), an MTL can be divided into a large number of sections of length Δz, each of which can be modeled as a lumped-element circuit referred to as PUL model. Figure A.9 depicts the PUL model for a three-conductor MTL[3].

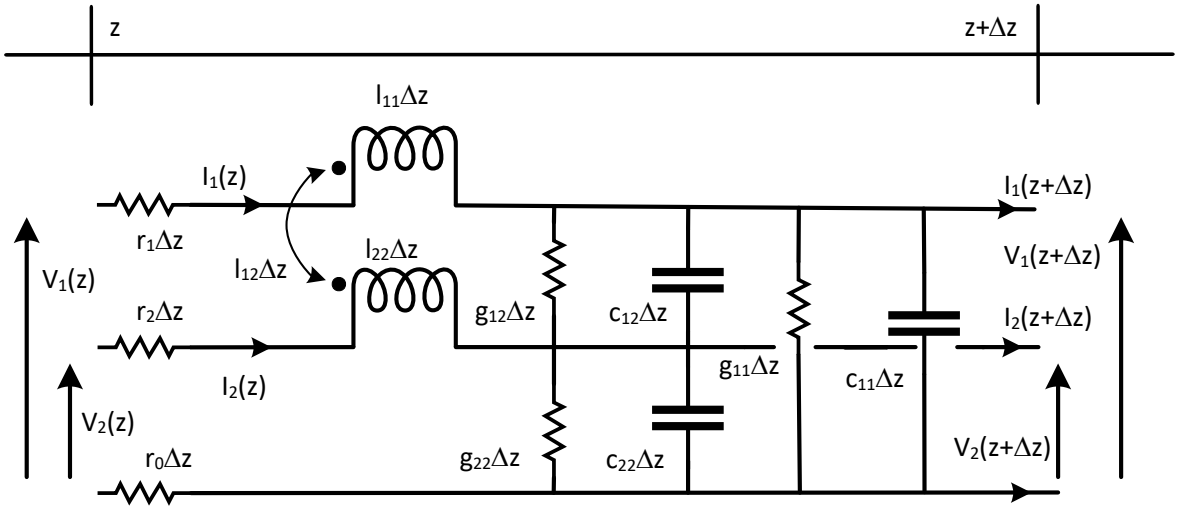

FIGURE A.9: PUL model of a three-conductor MTL, adapted from [82, Fig. 2.6]

[3]Fig. A.9 depicts a particular case of the (n+1)-conductor transmission line where $n = 2$. A generic (n+1)-conductor PUL model can be found in [82, Figure 2.6].

The PUL model is comprised of four kind of parameters which can be regarded as:

- The per-unit-length inductance, l_{ij}, represents the magnetic flux passing between the conductors due to the current on those conductors.
- The per-unit-length resitance, r_i, represents the losses due to be working with lossy conductors.
- The per-unit-length capacitance, c_{ij}, represents the displacement current flowing between the conductors in the transverse plane.
- The per-unit-length conductance, g_{ij}, represents the conduction current flowing between the conductors in the transverse plane.

The PUL model can be characterized by the following parameters:

- The inductance matrix $\mathbf{L}$, whose elements are

$$l_{ii} = \frac{\mu}{2\pi} \log\left(\frac{d_{i0}^2}{r_{w0} r_{wi}}\right),$$
$$l_{ij} = \frac{\mu}{2\pi} \log\left(\frac{d_{i0} d_{j0}}{d_{ij} r_{w0}}\right),$$

  where d_{ij} is the distance between centers of conductors i and j, r_{wi} is the radius of conductor i, and μ is the permeability of the conductor.

- The capacitance matrix $\mathbf{C}$, given by

$$\mathbf{C} = \mu\epsilon\mathbf{L}^{-1}, \tag{A.10}$$

  where ϵ is the permitivity of the dielectric.

- The conductance matrix $\mathbf{G}$, given by

$$\mathbf{G} = \omega \tan\delta \mathbf{C}, \tag{A.11}$$

where $\omega = 2\pi f$ is the angular frequency, $\tan\delta$ is the loss tangent that represents the dielectric loss.

- The resistance matrix $\mathbf{R}$, whose entries are given by

$$r_{ii} = r_i + r_0,$$

$$r_{ij} = r_0,$$

where r_i is

$$r_i = \begin{cases} \frac{1}{\sigma\pi r_{wi}^2} & r_{wi} < 2\delta \\ \frac{1}{2r_{wi}}\sqrt{\frac{\mu}{\pi\sigma}}\sqrt{f} & r_{wi} > 2\delta \end{cases},$$

and $\delta = \frac{1}{\sqrt{\pi f \mu \sigma}}$ is the skin depth.

The use of the PUL model to characterize an MTL requires some assumptions, being the most relevant ones:

- *Wide-separation approximation:* currents and charges are uniformly distributed around the wire peripheries, which implicitly assumes that wires are widely spaced. Even though it looks like this condition might not be met, it is shown that for a separation as small as 4 radii measured center-to-center (leaving space for only one other conductor to fit in between), closed expressions only deviate 5.3% from the exact value.

- *Uniform dielectric assumption:* this assumption is needed for the capacitance matrix $\mathbf{C}$ to be directly related to the inductance matrix $\mathbf{L}$ as in (A.10).

A.2.2 Transmission matrix of an MTL

Let us denote the following matrices associated to the PUL model, $\mathbf{Z} = \mathbf{R} + j\omega\mathbf{L}$ and $\mathbf{Y} = \mathbf{G} + j\omega\mathbf{C}$. The product $\mathbf{YZ}$ can be diagonalized as $\mathbf{YZ} = \mathbf{U}\boldsymbol{\gamma}^2\mathbf{U}^{-1}$, where $\boldsymbol{\gamma} = \text{diag}\,(\gamma_1, \gamma_2, \ldots, \gamma_n)$. Defining the characteristic impedance and admittance matrices as $\mathbf{Z}_C = \mathbf{Y}^{-1}\mathbf{U}\boldsymbol{\gamma}\mathbf{U}^{-1}$ and $\mathbf{Y}_C = \mathbf{Z}_C^{-1}$, respectively, and under certain assumptions

(given below), the $2n \times 2n$ transmission matrix at frequency f, $\mathbf{T}^{\text{line}}$, of an $(n+1)$-conductor MTL of length d can then be expressed as

$$\mathbf{T}^{\text{line}} = \begin{bmatrix} \mathbf{T}_{11}^{\text{line}} & \mathbf{T}_{12}^{\text{line}} \\ \mathbf{T}_{21}^{\text{line}} & \mathbf{T}_{22}^{\text{line}} \end{bmatrix}, \tag{A.12}$$

where

$$\mathbf{T}_{11}^{\text{line}} = \frac{1}{2}\mathbf{Y}^{-1}\mathbf{U}(\mathbf{e}^{\boldsymbol{\gamma} d} + \mathbf{e}^{-\boldsymbol{\gamma} d})\mathbf{U}^{-1}\mathbf{Y}, \tag{A.13}$$

$$\begin{aligned} \mathbf{T}_{12}^{\text{line}} &= -\frac{1}{2}\mathbf{Y}^{-1}\mathbf{U}\boldsymbol{\gamma}(\mathbf{e}^{\boldsymbol{\gamma} d} - \mathbf{e}^{-\boldsymbol{\gamma} d})\mathbf{U}^{-1} \\ &= -\frac{1}{2}\mathbf{Y}^{-1}\mathbf{U}\boldsymbol{\gamma}\mathbf{U}^{-1}[\mathbf{U}(\mathbf{e}^{\boldsymbol{\gamma} d} - \mathbf{e}^{-\boldsymbol{\gamma} d})\mathbf{U}^{-1}] \\ &= -\frac{1}{2}\mathbf{Z}_C[\mathbf{U}(\mathbf{e}^{\boldsymbol{\gamma} d} - \mathbf{e}^{-\boldsymbol{\gamma} d})\mathbf{U}^{-1}], \end{aligned} \tag{A.14}$$

$$\begin{aligned} \mathbf{T}_{21}^{\text{line}} &= -\frac{1}{2}\mathbf{U}(\mathbf{e}^{\boldsymbol{\gamma} d} - \mathbf{e}^{-\boldsymbol{\gamma} d})\boldsymbol{\gamma}^{-1}\mathbf{U}^{-1}\mathbf{Y} \\ &= -\frac{1}{2}[\mathbf{U}(\mathbf{e}^{\boldsymbol{\gamma} d} - \mathbf{e}^{-\boldsymbol{\gamma} d})\mathbf{U}^{-1}]\mathbf{U}\boldsymbol{\gamma}^{-1}\mathbf{U}^{-1}\mathbf{Y} \\ &= -\frac{1}{2}[\mathbf{U}(\mathbf{e}^{\boldsymbol{\gamma} d} - \mathbf{e}^{-\boldsymbol{\gamma} d})\mathbf{U}^{-1}]\mathbf{Y}_C, \end{aligned} \tag{A.15}$$

$$\mathbf{T}_{22}^{\text{line}} = \frac{1}{2}\mathbf{U}(\mathbf{e}^{\boldsymbol{\gamma} d} + \mathbf{e}^{-\boldsymbol{\gamma} d})\mathbf{U}^{-1}, \tag{A.16}$$

where the matrix exponential is defined as $\mathbf{e}^{-\boldsymbol{\gamma} d} = \text{diag}\left(e^{\gamma_1 d}, e^{\gamma_2 d}, \ldots, e^{\gamma_n d}\right)$.

This solution for the MTL equations are only valid under some assumptions. The most relevant one being the *quasi-TEM assumption*. For this to hold, conductor losses must be small and the cross-sectional dimension of the lines must be much less than a wavelength. This holds due to the high conductivity of metals used in PLC (usually copper) and the radii of such conductors being a few millimeters long against the approximate 3-meter length of electric waves at 100 MHz (highest frequency used in this thesis).

Appendix B

MTL Simulator Validation

The goal of this appendix is to validate the simulator that has been implemented using the expressions shown in Appendix A. To that end, the following three-step approach will be followed:

1. *Compare the results given by the implemented simulator to the analytical solution given in [82, Sec. 6.1.].* The latter provides direct and crosstalk voltage gains but is only valid for a very specific lossless structure.

2. *Select a circuit simulation tool that allows computing the solution to more complex MTL structures.* Since the previous analytical solution only applies to a lossless line and a very specific structures, an additional approach is needed to test the simulator in a wider range of scenarios. This can be achieved by taking advantage of the PUL model of MTL and implementing them as a large set of lumped-element cells that model a short line segment. To this end, the circuit simulation tool called *Proteus ISIS* has been employed[1] [83]. Since the PUL model requires the line segment to be electrically short at the considered wavelength, the relation between the number of line segments and the accuracy of the results has been assessed in the layout for which the analytical solution is known.

3. *Compare the results given by the implemented simulator to the ones given by the circuit simulation tool.* Now that both the lumped-element implementation and

[1]The software version used for this analysis is Release 7.7.

our MTL-based simulator have been validated for a given lossless line, their results are compared in a larger number of layouts and line conditions, i.e., lossless and lossy lines. To this end, the basic relations used in the proposed simulator have been assessed: frequency response of a loaded MTL; input impedance of a loaded MTL; transmission matrix of a parallel load.

In all cases, the assessment is accomplished in three-conductor test scenarios. The convenience of testing on three-conductor structures is twofold: the channel simulator in [41] uses three-conductor transmission lines and three-conductor models are the simplest MTL scenarios, thus keeping computation as simple as possible.

B.1 Frequency response of a loaded MTL

This section firstly compares the analytical solution in [82, Sec. 6.1.], corresponding to a lossless MTL, to the results obtained with the MTL-based simulator implemented using the expressions given in Appendix A and to the ones given by the *Proteus ISIS* circuit simulator. The assessment is then extended to lossy lines. However, since no analytical expression Afterwards, results obtained with the proposed MTL-based simulator and *Proteus ISIS* are compared in a lossy line.

B.1.1 Validation in a lossless line

Let us consider the three-conductor lossless transmission line (i.e., r_i and g_{ij} in the model depicted in Fig. A.9 are zero) depicted in Fig. B.1. The modulus of the crosstalk voltage $H_{XT}(f) = V_{FE}(f)/V_S(f)$, given by Eq. (6.17b) in [82], is calculated in the three different scenarios whose parameters are shown in Table B.1. The parameters depicted in the table are: Length, length of the transmission line that connects transmitting and receiving ends; Cable section, which is the area of the cross section of the wiring[2] used to model the transmission line; Sep. cond. i-j, which

[2]It is assumed that all conductors that comprise the line have the same cross section.

represents the separation between conductors i and j; Conductivity, the conductity of the conductors; Loss tangent, a loss factor associated to the existing dielectric among conductors; and, lastly, R_S, R_L, R_{FE}, and R_{NE} (depicted in Fig. B.1), which represent the source, load, far-end and near-end loads, respectively.

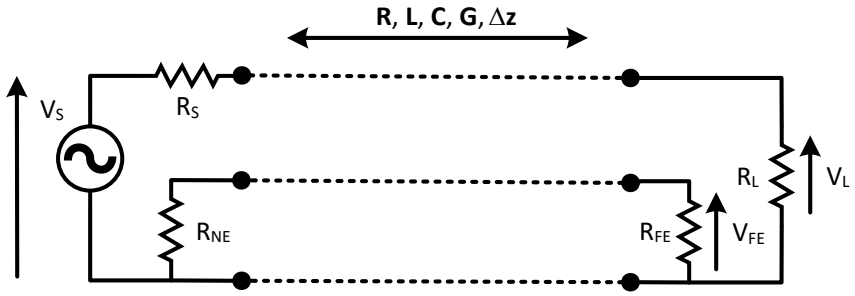

FIGURE B.1: Three-conductor line dimensions and terminal characterization as in [82, Sec. 6.1.].

	Scenario		
Parameter	1	2	3
Length [m]	2.7	5.4	10.8
Cable section [mm^2]	4	6	10
R_S [Ω]	100	50	50 + 25i
R_L [Ω]	100	150	100 - 50i
R_{FE} [Ω]	100	100	50 + 100i
R_{NE} [Ω]	100	200	75 - 25i
Sep. cond. 1-2 [mm] (*)	5.64 (5)	5.53 (4)	5.35 (3)
Sep. cond. 1-0 [mm] (*)	5.64 (5)	4.16 (3)	12.49 (7)
Sep. cond. 2-0 [mm] (*)	5.64 (5)	6.91 (5)	14.27 (8)
Conductivity [MS/m] (**)	58	58	58
Loss tangent (**)	0.025	0.025	0.025

TABLE B.1: Parameters of the three scenarios used to configure the structure depicted in Fig. B.1. (*) In the Sep. cond. category, the number in parentheses is the distance expressed in multiples of the conductor radius. (**) Only applicable to lossy scenarios. In lossless scenarios these values are infinity and zero, respectively.

Analytic solution vs MTL-based simulator

Figs. B.2 depicts the crosstalk voltage gain in the frequency up to 100 MHz and B.3 the relative difference between the values obtained with the MTL-based simulator

and the analytical ones. As seen, both are effectively equal in the three scenarios, yielding relative difference values below -250 dB.

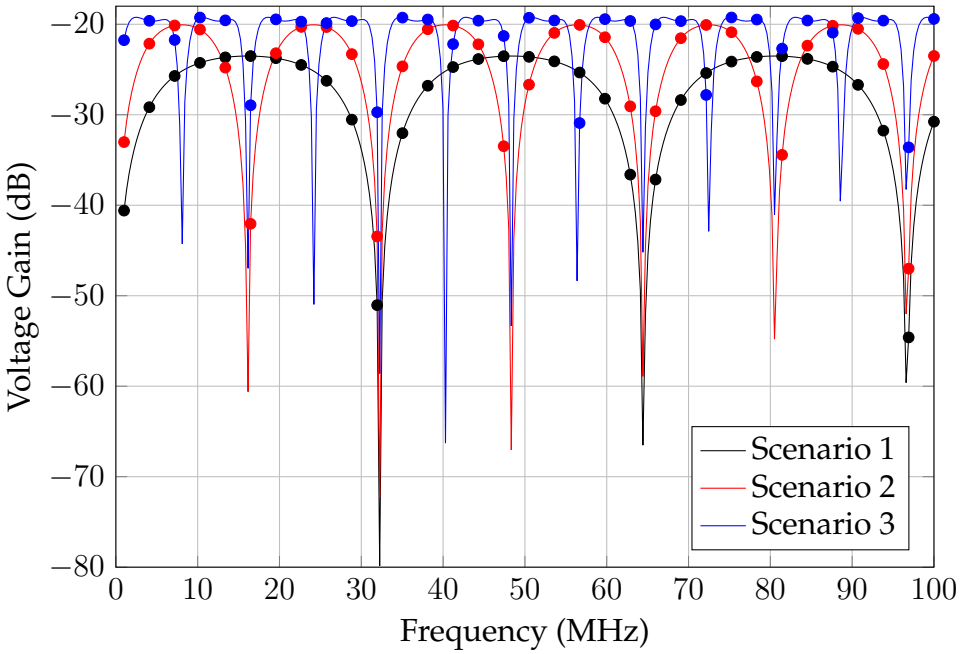

FIGURE B.2: Amplitude of the crosstalk voltage gain obtained with the MTL-based simulator (solid line) and the analytic expression (markers) in the structure depicted in Fig. B.1 configured with the parameters of the Scenario 1 in Table B.1.

Proteus ISIS solution vs MTL-based simulator

In order to use *Proteus ISIS* to compute the crosstalk voltage gain of the three-conductor lossless transmission line in Fig. B.1 a lumped element model of this transmission line is defined by cascading the basic cell of the PUL model shown in Fig. A.9 N times. Since lumped element models are valid only for $\Delta z \ll \lambda$, being Δz the length of the line and λ the wavelength at the considered frequency, the number of cells to be cascaded depends on the length of the line to be simulated. As the number of cells that can be employed in the available version of *Proteus ISIS* is limited, results are computed only for the shorter scenario shown in Table B.1, i.e., Scenario 1.

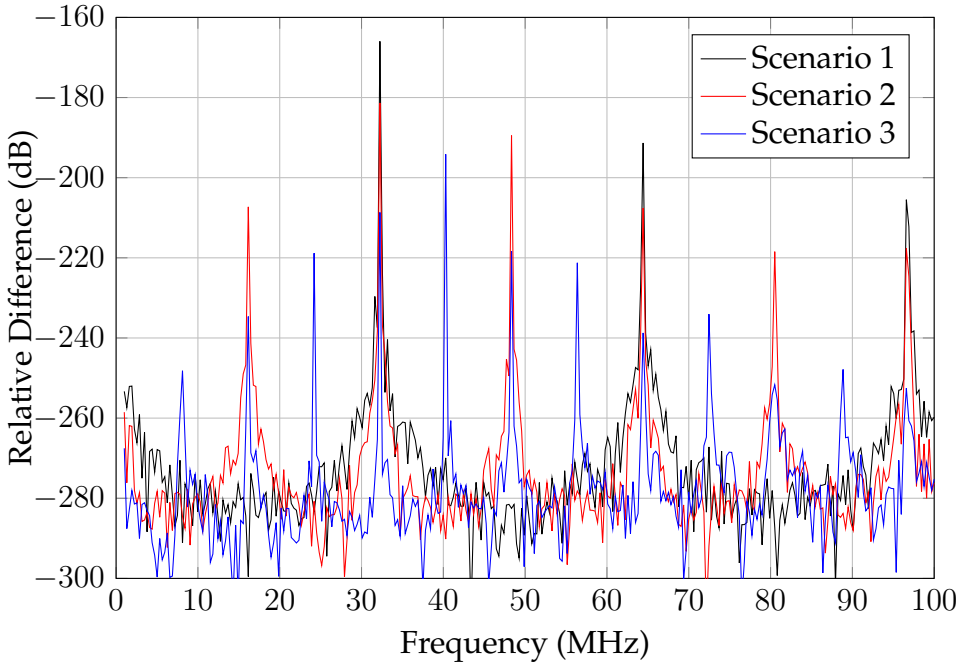

FIGURE B.3: Relative difference between the crosstalk voltage gain values given by the MTL-based simulator and the analytic expression depicted in Fig. B.2. The relative difference of two complex magnitudes is defined as $|A - B|/|B|$, where $|\cdot|$ is the absolute value operator.

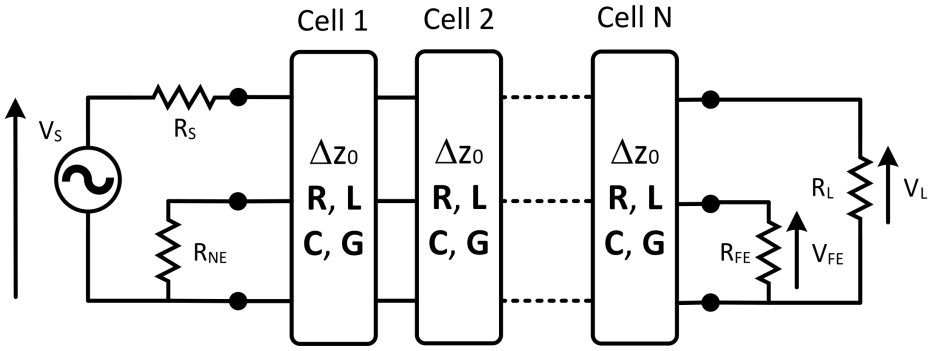

FIGURE B.4: Lumped element model of the three-conductor transmission line consisting of N cascaded cells as the one in Fig. A.9.

Fig. B.5 shows the direct voltage gain, defined as $|H_D(f)| = \left|V_L(f)/V_S(f)\right|$, and the crosstalk one obtained with *Proteus ISIS* and the MTL-based simulator. Similarly, Fig. B.6 depicts the relative difference between both results. As seen, the distance between the lumped element simulation and the MTL-based one grows with frequency. This is due to the enlarging of the electrical length of each segment as frequency increases, since the relative difference reduces as the number of segments increases.

At a given frequency, f, a conductor segment of length Δz is said to be electrically short when it is much shorter than the wavelength λ. In practice, the latter relation is usually interpreted as $\Delta z < \lambda/10$. Since $\lambda = \frac{v_p c_0}{f}$, where v_p is the velocity factor and c_0 is the speed of light in vacuum, assuming $v_p = 0.66$, at 100 MHz, a conductor must be shorter than 0.2 meters to be electrically short. For the previous scenario, where the line is 2.7 meter long, this means the line must be split into at least 14 equally spaced segments for each of them to be considered electrically short. Similarly, at 50 MHz, 7 segments would be needed, whereas as few as 2 segments would suffice at 10 MHz. However, Fig.B.6 shows that while at 10 MHz using a number of segments that is $9/2 = 4.5$ times larger than the one given by the condition $\Delta z < \lambda/10$ yields a relative difference of -100 dB in the direct voltage gain, at 100 MHz, using a number of segments that is also $63/14 = 4.5$ times the one given by the aforementioned condition gives a much larger relative difference (about -40 dB). Moreover, increasing the number of segments to $81/14 = 5.7$ times yields a very modest reduction in the relative difference. It is also important to note that the relative error is different in each voltage gain (direct and crosstalk). These results agree with the ones given in [84], which also show that the relative difference depends also on the PUL parameters of the considered transmission line.

Hence, presented results suggest that the difference between the MTL-based simulator and *Proteus ISIS* are due to the limited number of cells. However, the modest reduction in the relative difference obtained when increasing the latter from 63 to 81 indicates that improving the obtained accuracy requires simulating circuits with thousands of elements[3], which is very cumbersome. Finally, it is worth noting that the relative difference depicted in Fig. B.6 is expected to be lower, the larger the number of segments (shorter segments), which holds for all cases except for $N = 63$ and $N = 81$ below 30 MHz. This must be due to the circuit simulation tool *Proteus ISIS* since the accuracy of the MTL for this very same lossless scenario was already

[3]Note that the 81-segment scenario has required simulating circuits with 891 lumped elements, as every segment is implemented in *Proteus ISIS* using 11 lumped elements (five resistors, three coupled inductors and three capacitors).

proven as shown in Fig. B.2 and Fig. B.3. Moreover, in this case ($N = 63$ and $N = 81$ below 30 MHz), the relative difference is always lower than -60 dB so *Proteus ISIS* can be deemed a suitable tool to validate the MTL simulator expressions.

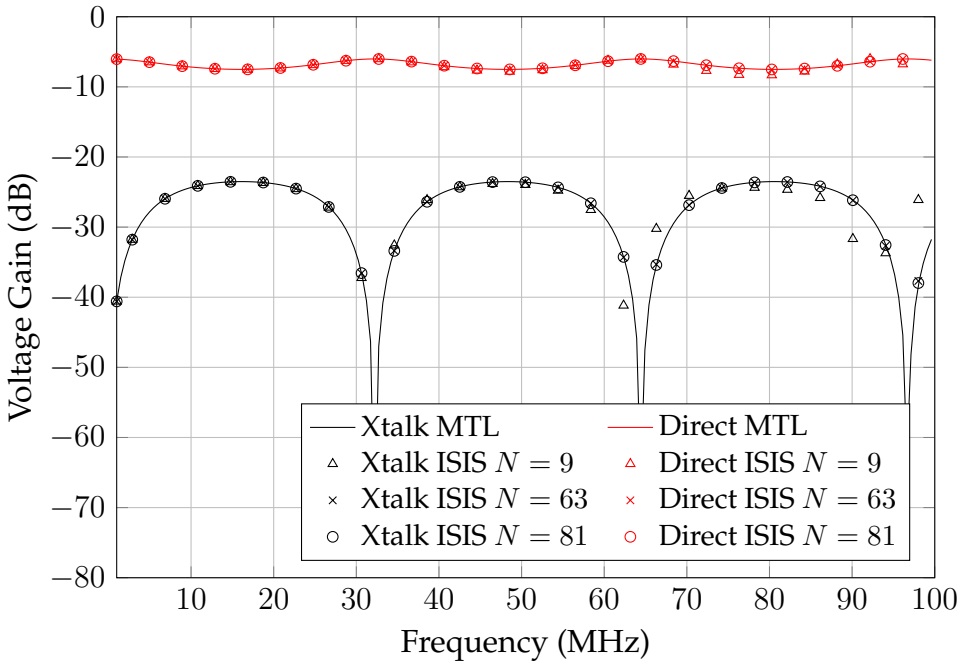

FIGURE B.5: Crosstalk and direct voltage gain between the solutions given by *Proteus ISIS* and the MTL-based simulator in the structure shown in Fig.B.1. The MTL is a lossless one with the parameters of the Scenario 1 in Table B.1. *Proteus ISIS* simulations have been done by splitting the transmission line in $N = 9$ (triangle), $N = 63$ (cross), and $N = 81$ (circle) segments, respectively.

B.1.2 Validation in a lossy line

The direct and crosstalk voltage gains given by the proposed MTL-based simulator and *Proteus ISIS* are now compared in a lossy line as the one of Scenario 1 in Table. B.1) but with $\sigma = 58 \cdot 10^6$ Siemens (copper conductivity) and $\tan(\delta) = 0.025$.

Fig. B.7 and Fig. B.8 show the voltage gains and their relative difference, respectively. Results shown in the latter figure are very similar to the ones obtained for the lossless line case. Hence, the same comments made for Fig. B.6 are also applicable here.

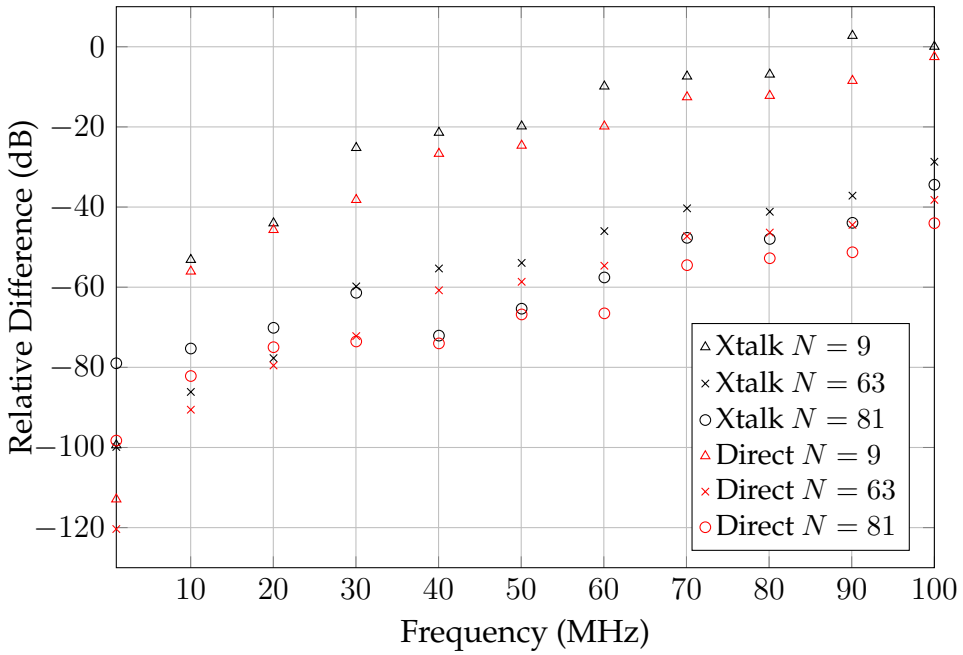

FIGURE B.6: Relative difference between the crosstalk and direct voltage gain values given by the MTL-based simulator and *Proteus ISIS* in the structure shown in Fig.B.5

.

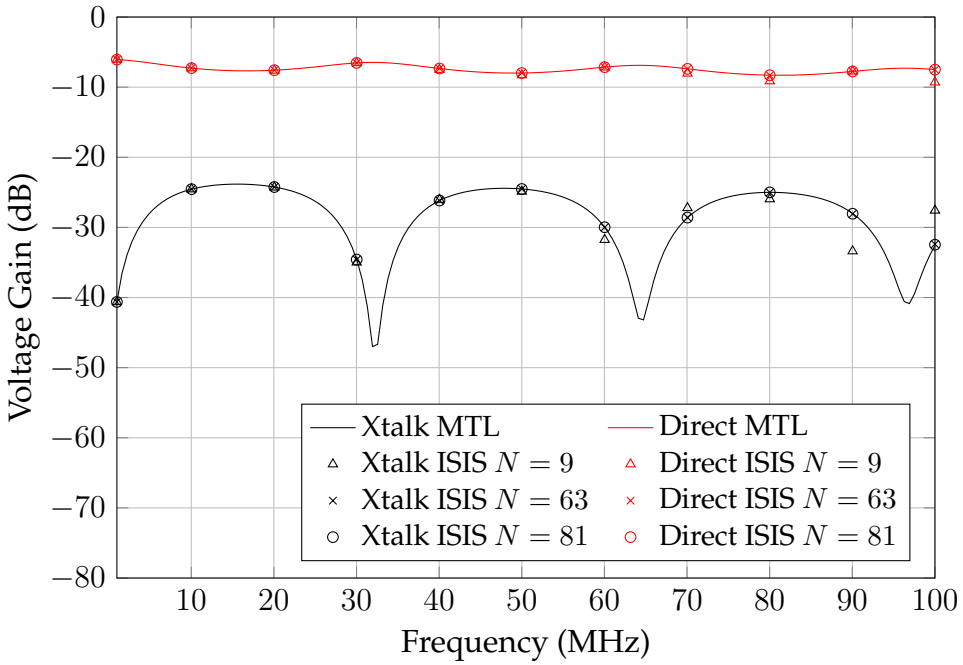

FIGURE B.7: Crosstalk and direct voltage gain between the solutions given by *Proteus ISIS* and the MTL-based simulator in the structure shown in Fig.B.1. The MTL is a lossy one with the parameters of the Scenario 1 in Table B.1. The implementation in *Proteus ISIS* divides the overall line into $N = 9$ (triangle), $N = 63$ (cross), and $N = 81$ (circle) segments, respectively.

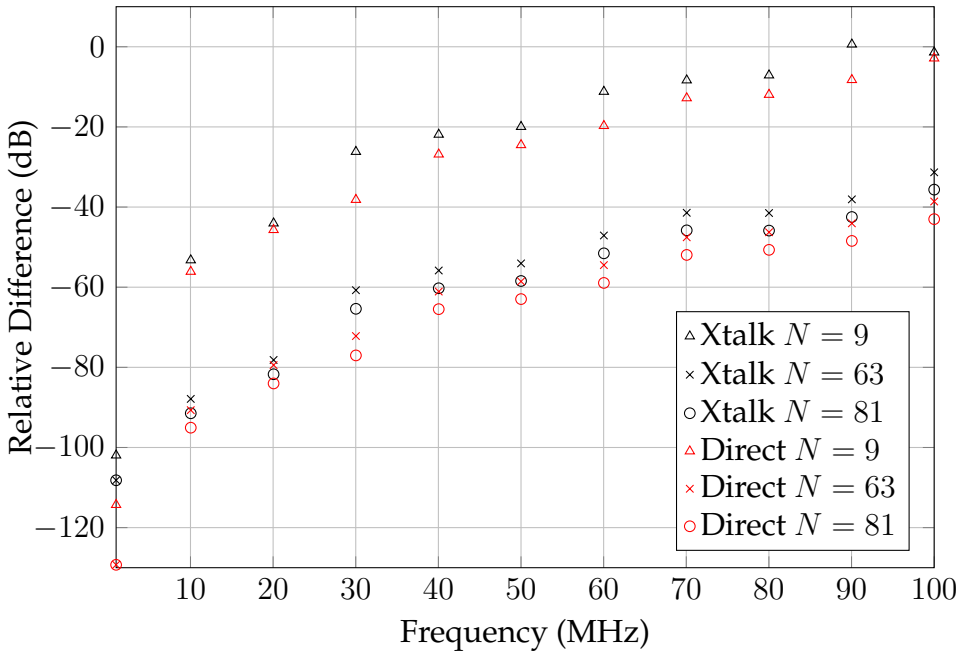

FIGURE B.8: Relative difference between the crosstalk and direct voltage gain values given by the MTL-based simulator and *Proteus ISIS* in the structure shown in Fig.B.7.

B.2 Validation of the input impedance matrix of a loaded line

In this section, *Proteus ISIS* is used to validate the implementation made in the MTL-based simulator of the expressions of the input impedance matrix for delta-style loads and loaded MTLs given in Section A.1.2.

The validity of the expression given in Eq. (A.7) for the input impedance of the loaded MTL depicted in Figure A.4 is assessed in the lossy version (with $\sigma = 58 \cdot 10^6$ Siemens and $\tan(\delta) = 0.025$) of the MTL defined in Scenario 1 of Table. B.1. This line is implemented in *Protesus ISIS* as the cascade of $N = 81$ segments. The values for the elements comprising the load in Fig. B.9 can be found in Table B.2. The parameter z_{12}^{in} is not shown since, due to the reciprocity theorem of passive networks, it is equal to z_{21}^{in}.

Fig. B.10 and Fig. B.11 show the absolute value of the input impedance matrix elements computed with the MTL-based simulator and *Proteus ISIS* and the relative

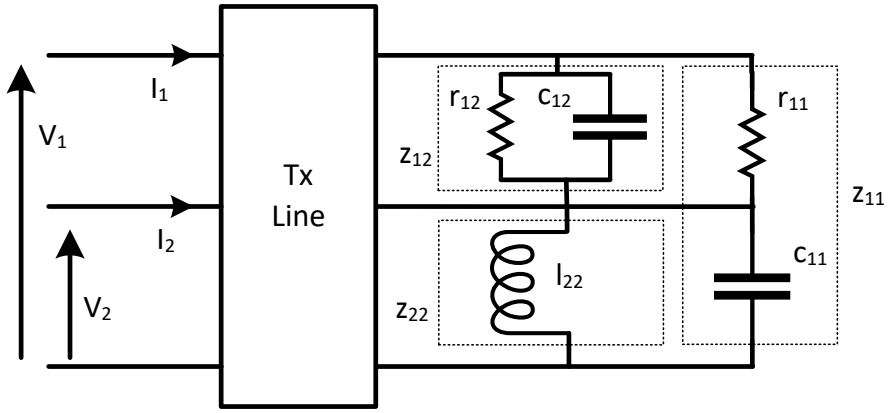

FIGURE B.9: Model of the loaded lossy MTL under test. Parameters of the MTL correspond to the Scenario 1 in Table. B.1 with $\sigma = 58 \cdot 10^6$ Siemens and $\tan(\delta) = 0.025$.

Impedance	Values
z_{11}	$r_{11} = 100\ \Omega$, $c_{11} = 4$ nF
z_{22}	$l_{22} = 1\ \mu$H
z_{12}	$r_{12} = 250\ \Omega$, $c_{12} = 65$ pF

TABLE B.2: Values of the elements of the delta-style load shown in Fig. B.9.

error between them, respectively. As seen, Fig. B.11 shows that both approaches provide results almost equal results, since relative difference values are around -120 dB.

B.3 Validation of the transmission matrix of a parallel load

Similarly to the previous section, this analysis is focused on the validation, via the circuit simulation tool *Proteus ISIS*, of the expressions of the transmission matrix of a parallel load consisting on a loaded MTL given in Section A.1. Note that, as expression (A.8) point out, submatrices $\mathbf{T}_{11}$, $\mathbf{T}_{22}$ and $\mathbf{T}_{12}$ only include parameters that are either one or zero. Hence, the elements of submatrix $\mathbf{T}_{21}$ will be shown in the following figures.

In this section the transmission matrix of a parallel MTL loaded with the delta-style one given in Table B.2 is computed using the MTL-based simulator and *Proteus*

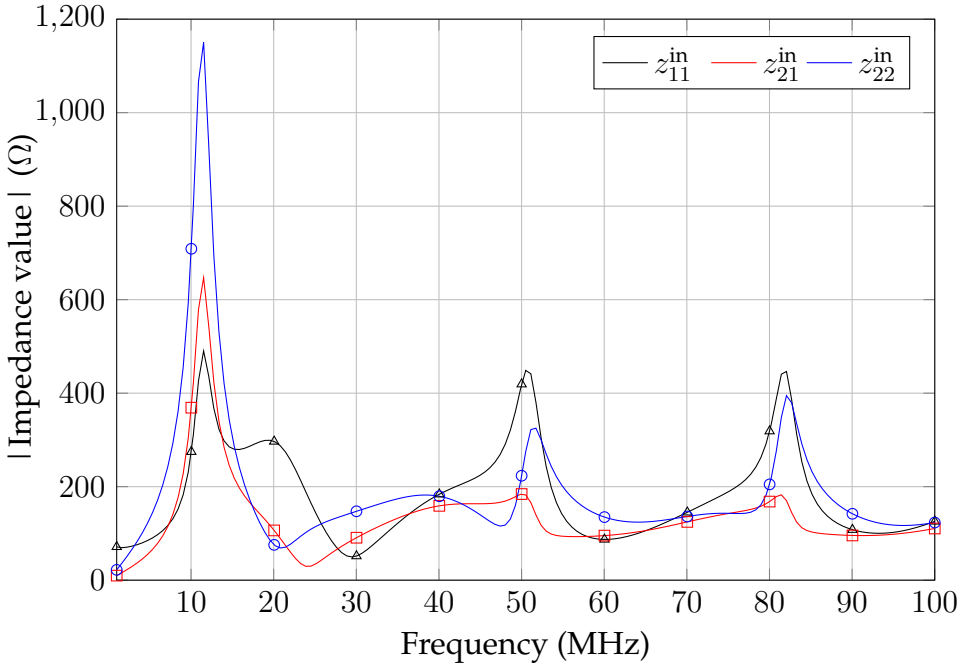

FIGURE B.10: Absolute value of the elements of the impedance matrix corresponding to the loaded line in Fig. B.9 as given by the MTL-based simulator (solid line) and *Proteus ISIS* (markers). In the latter, the line is implemented by cascading $N = 81$ segments.

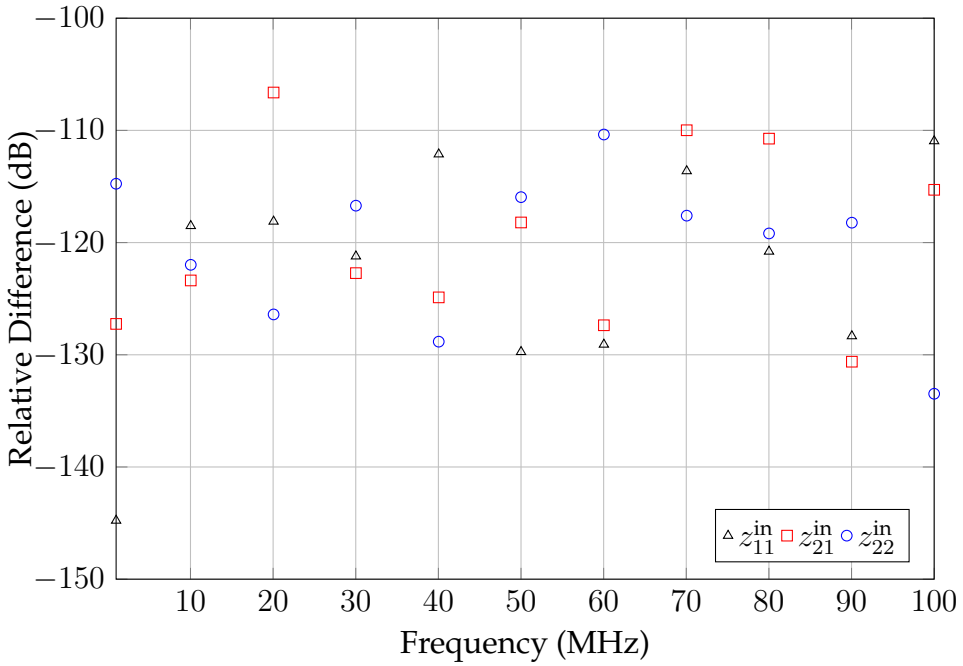

FIGURE B.11: Relative difference between the values of the elements of the input impedance matrix computed by the MTL-based simulator and *Proteus ISIS* displayed in Fig. B.10.

ISIS. The MTL is the lossy version of Scenario 1 in Table B.1. To this end, the scenario depicted in Fig. B.12 has been implemented in *Proteus ISIS* using $N = 81$ cascaded segments for the circuital implementation of the transmission line.

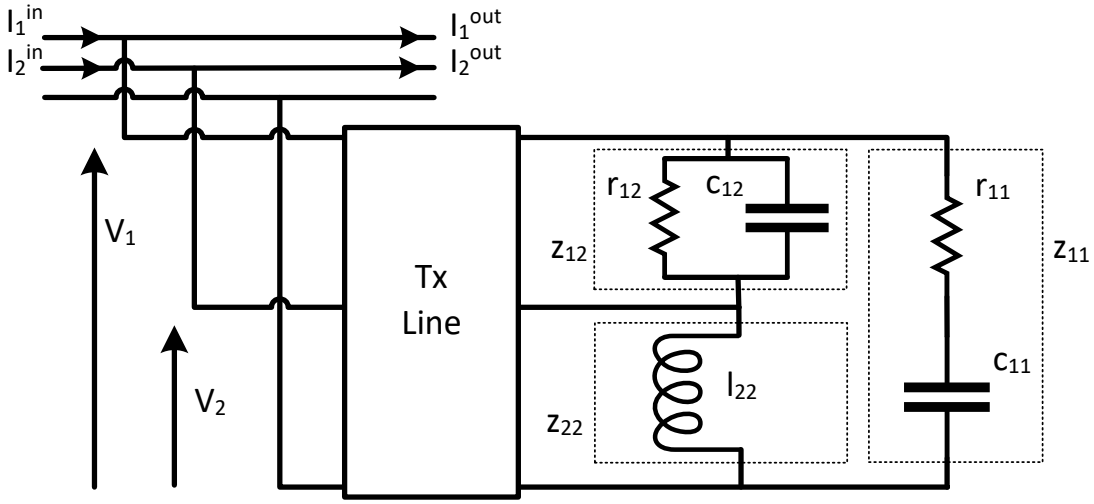

FIGURE B.12: Model of the parallel loaded MTL under test.

Fig. B.13 shows the absolute value of the elements of the submatrix $\mathbf{T}_{21}$ given by the MTL-based simulator and *Proteus ISIS*, whereas Fig. B.14 depicts the relative difference between both. As seen, both yield essentially the same values, as their relative difference is lower than -90 dB in the whole frequency band. The parameter t_{41} is not shown because, according to (A.8), it is equal to t_{32}.

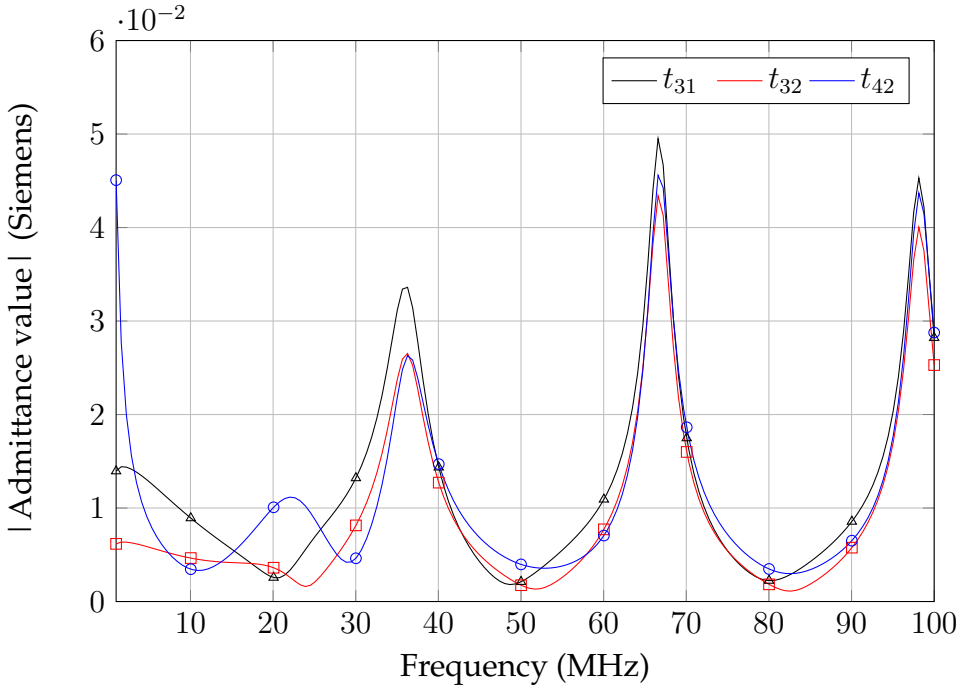

FIGURE B.13: Absolute value of the elements of the transmission matrix corresponding to the structure shown in Fig. B.12 as given by the MTL-based simulator and *Proteus ISIS*. The MTL is implemented in *Proteus ISIS* using $N = 81$ segments.

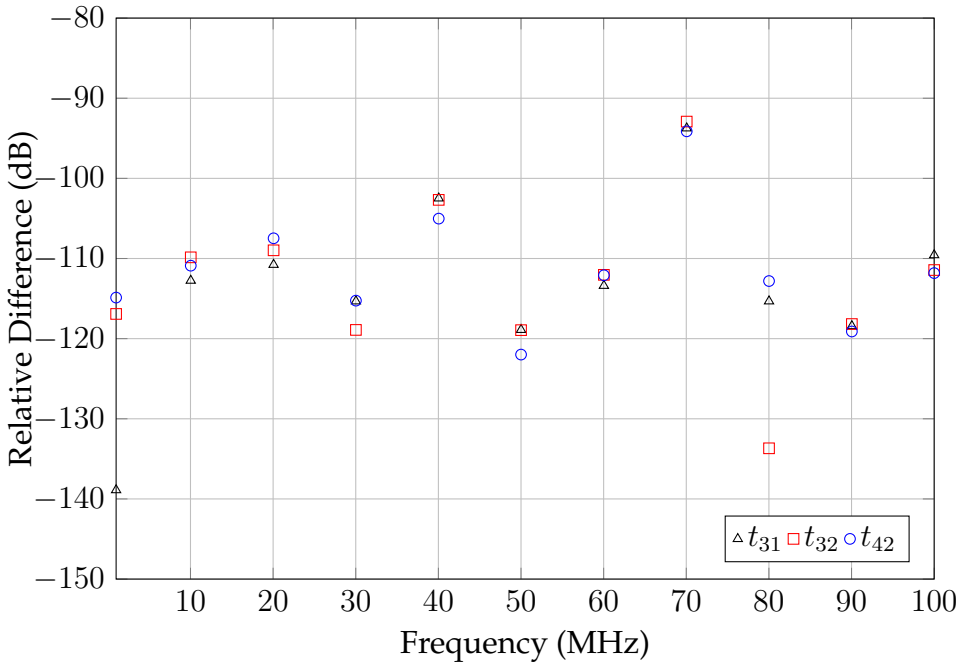

FIGURE B.14: Relative difference between the values of the elements of the transmission matrix given by the MTL-based simulator and *Proteus ISIS* displayed in Fig. B.13.

Bibliography

[1] "IEEE Standard for Ethernet," *IEEE Std 802.3-2015 (Revision of IEEE Std 802.3-2012)*, pp. 1–4017, Mar. 2016.

[2] "IEEE Standard for Information Technology–Telecommunications and Information Exchange between Systems - Local and Metropolitan Area Networks–Specific Requirements - Part 11: Wireless LAN Medium Access Control (MAC) and Physical Layer (PHY) Specifications," *IEEE Std 802.11-2020 (Revision of IEEE Std 802.11-2016)*, pp. 1–4379, 2021.

[3] P. A. Brown, "Power line communications: past, present, and future," in *IEEE International Symposium on Power Line Communications and Its Applications (ISPLC)*, Jan. 1999, pp. 1–8.

[4] J. J. Fahie, "Edward Davy," *The Electrician*, pp. 181–227, Jul. 1883.

[5] J. Routin and C. Brown, "Power line signaling electricity meters," *UK Patent Office, British Patent No. 24833, 1897*, 1897.

[6] K. Dostert, *Powerline Communications* (Prentice Hall communications engineering and emerging technologies series). Prentice Hall PTR, 2001.

[7] Broadridge, R., "Power-line models and networks," in *IEE 4th International Conference on Metering Applications and Tariffs for Electricity Supply IEE Conf. Publ.*, London, UK, 1984, pp. 294–296.

[8] *About the X10 Home Automation Technology - Reference to the X10 home page*, `https://rb.gy/en4odt`.

[9] T. Sheppard, "Mains communications - a practical metering system," in *Proceedings of the 7th International Conference on Metering Applications and Tariffs for Electricity Supply*, Nov. 1992, pp. 223–227.

[10] L. Lampe, A. M. Tonello, and T. G. Swart, Eds., *Power line communications: principles, standards and applications from multimedia to Smart Grid*, Second Ed. Wiley, Jun. 2016.

[11] *HomePlug AV Specification Version 1.1*, HomePlug Alliance, Specification. [Online]. Available: https://rb.gy/eymqr3, Feb. 2007.

[12] *Universal Powerline Association Specification. Digital Home System v1.0*, Universal Powerline Association Specification, Feb. 2006.

[13] *Unified high-speed wireline-based home networking transceivers - multiple input/multiple output specification*, ITU-T Recommendation G.9963, International Telecommunications Union, Dec. 2011.

[14] *IEEE Standard for Broadband over Power Line Networks: Medium Access Control and Physical Layer Specifications*, IEEE Std 1901-2020.

[15] *HomePlug AV Specification Version 2.1*, HomePlug Alliance, Specification. [Online]. Available: https://bit.ly/39YvjXB, Feb. 2014.

[16] S. Galli, A. Scaglione, and Z. Wang, "For the grid and through the grid: The role of power line communications in the Smart Grid," *Proceedings of the IEEE*, vol. 99, no. 6, pp. 998–1027, Jun. 2011.

[17] *Open Data Communication in Building Automation, Controls and Building Management - Control Network Protocol*, ISO/IEC 14908, Standard, 2008.

[18] *Distribution Automation Using Distribution Line Carrier Systems - Part 5-2: Lower Later Profiles - Frequency Shift Keying (S-FSK) Profile*, IEC Std. 61334-5-2, Standard, 1998.

[19] *Distribution Automation Using Distribution Line Carrier Systems - Part 5-1: Lower Later Profiles - Spread Frequency Shift Keying (S-FSK) Profile*, IEC Std. 61334-5-1, Standard, 2001.

[20] *Powerline Related Intelligent Metering Evolution (PRIME)*, `http://www.prime-alliance.org/`, Reference to the PRIME Alliance web page.

[21] *G3-PLC: Open Standard for SmartGrid Implementation*, `https://rb.gy/cllt5i`, Reference to the Specifications and User Guidelines and Application Notes of the G3-Alliance.

[22] "IEEE Standard for Medium Frequency (less than 12 MHz) Power Line Communications for Smart Grid Applications," *IEEE Std 1901.1-2018*, pp. 1–192, 2018.

[23] *Huawei and IEEE P1901.1 Working Group Jointly Celebrate Publication of PLC-IoT Standard*, `https://rb.gy/bpixy8`, [Press release issued by Huawei. Last accessed 30-September-2023], 2018.

[24] *G.hn Overview - Reference to the HomeGrid Forum web page*, `https://homegridforum.org/`.

[25] F. J. Cañete, L. Díez, J. A. Cortés, and J. T. Entrambasaguas, "Broadband Modelling of Indoor Power-Line Channels," *IEEE Transactions on Consumer Electronics*, vol. 48, no. 1, pp. 175–183, Feb. 2002.

[26] F. J. Cañete, J. A. Cortés, L. Díez, and J. T. Entrambasaguas, "Analysis of the cyclic short-term variation of indoor power line channels," *IEEE Journal on Selected Areas on Communications*, vol. 24, no. 7, pp. 1327–1338, Jul. 2006.

[27] J. Cortés, L. Diez, F. J. Cañete Corripio, and J. Sanchez-Martinez, "Analysis of the indoor broadband power-line noise scenario," *IEEE Transactions on Electromagnetic Compatibility*, vol. 52, pp. 849 –858, Dec. 2010.

[28] *Unified high-speed wireline-based home networking transceivers - System architecture and physical layer specification*, ITU-T Recommendation G.9960, International Telecommunications Union, Jul. 2015.

[29] *Data Link Layer (DLL) for Unified High-Speed Wire-Line Based Home Networking Transceivers*, ITU-T Recommendation G.9961, International Telecommunications Union, Jun. 2010.

[30] *Unified high-speed wireline-based home networking transceivers - Power spectral density specification*, ITU-T Recommendation G.9964, International Telecommunications Union, Dec. 2011.

[31] *Coexistence Mechanism for Wireline Home Networking Transceivers*, ITU-T Rec. G.9972. International Telecommunications Union, Jun. 2010.

[32] J. A. Cortés, F. J. Cañete, M. Toril, E. Martos-Naya, J. Poncela, L. Díez, and A. Garía, "Feasibility study of power line communications for backhauling outdoor small cells," *IEEE Access*, vol. 9, pp. 30 135–30 153, Feb. 2021.

[33] M. Girotto and A. M. Tonello, "EMC regulations and spectral constraints for multicarrier modulation in PLC," *IEEE Access*, vol. 5, pp. 4954–4966, Mar. 2017.

[34] *The impact of power line high data rate telecommunication systems on radiocommunication systems below 470 MHz*, ITU-R Recommendation SM.1879-2, International Telecommunications Union, Aug. 2013.

[35] L. T. Berger, A. Schwager, P. Pagani, and D. M. Schneider, "MIMO Power Line Communications," *IEEE Communications Surveys Tutorials*, vol. 17, no. 1, pp. 106–124, Jan. 2015.

[36] *Power line communication apparatus used in low-voltage installations - Radio disturbance characteristics - Limits and methods of measurement - Part 1: Apparatus for in-home use*, EN 50561-1, Comité Européen de Normalisation Electrotechnique (CENELEC), Oct. 2013.

[37] *Power line communication apparatus used in low-voltage installations - Radio disturbance characteristics - Limits and methods of measurement - Part 3: Apparatus operating above 30 MHz*, EN 50561-3:2016, Comité Européen de Normalisation Electrotechnique (CENELEC), 2016.

[38] *Title 47 of the code of federal regulations (CFR), technical report 47 CFR. 15*, Federal Communications Commission, Jul. 2008.

[39] L. Yonge, J. Abad, K. Afkhamie, L. Guerrieri, S. Katar, H. Lioe, P. Pagani, R. Riva, D. M. Schneider, and A. Schwager, "An overview of the HomePlug AV2 technology," *Journal of Electrical and Computer Engineering*, vol. 2013, pp. 1–20, 2013.

[40] A. Goldsmith, *Wireless Communications*. New York: Cambridge University Press, 2005.

[41] J. A. Corchado, J. A. Cortés, F. J. Canete, and L. Díez, "An MTL-Based Channel Model for Indoor Broadband MIMO Power Line Communications," *IEEE Journal on Selected Areas in Communications*, vol. 34, no. 7, pp. 2045–2055, Jul. 2016.

[42] J. A. Corchado, J. A. Cortés, F. J. Canete, A. Arregui, and L. Díez, "Analysis of the Spatial Correlation of Indoor MIMO PLC Channels," *IEEE Communications Letters*, vol. 21, no. 1, pp. 40–43, Jan. 2017.

[43] J. A. Cortés, J. A. Corchado, F. J. Canete, and L. Díez, "Analysis and Exploitation of the Noise Correlation in MIMO Power Line Communications in the FM Band," *IEEE Communications Letters*, vol. 22, no. 3, pp. 566–569, Mar. 2018.

[44] A. Schwager, D. Schneider, W. Bäshlin, A. Dilly, and J. Speidel, "MIMO PLC: Theory, Measurements and System Setup," in *Proceedings of the IEEE International Symposium on Power Line Communications and its Applications*, 2011, pp. 48–53.

[45] A. Schwager, W. Bäschlin, H. Hirsch, P. Pagani, N. Weling, and J. L. Gonzalez Moreno, "European MIMO PLT field measurements: Overview of the ETSI STF410 campaign & EMI analysis," in *Proceedings of the IEEE International Symposium on Power Line Communications and Its Applications (ISPLC)*, 2012, pp. 298–303.

[46] D. Schneider, A. Schwager, W. Bäshlin, and P. Pagani, "European MIMO PLC field measurements: Channel analysis," in *Proceedings of the IEEE International Symposium on Power Line Communications and its Applications*, 2012, pp. 304–309.

[47] D. Veronesi, R. Riva, P. Bisaglia, F. Osnato, K. Afkhamie, A. Nayagam, D. Rende, and L. Yonge, "Characterization of in-home MIMO power line channels," in *Proceedings of the IEEE International Symposium on Power Line Communications and Its Applications (ISPLC)*, 2012, pp. 42–47.

[48] P. Pagani, R. Hashmat, A. Schwager, D. Schneider, and W. Bäshlin, "European MIMO PLC field measurements: Noise analysis," in *Proceedings of the IEEE International Symposium on Power Line Communications and its Applications*, 2012, pp. 310–315.

[49] D. Rende, A. Nayagam, K. Afkhamie, L. Yonge, R. Riva, D. Veronesi, F. Osnato, and P. Bisaglia, "Noise Correlation and Its Effect on Capacity of In-home MIMO Power Line Channels," in *Proceedings of the IEEE International Symposium on Power Line Communications and Its Applications (ISPLC)*, 2011, pp. 60–65.

[50] S. Galli and T. C. Banwell, "A deterministic frequency-domain model for the indoor power line transfer function," *IEEE Journal on Selected Areas in Communications*, vol. 24, no. 7, pp. 1304–1316, Jul. 2006.

[51] F. Versolatto and A. M. Tonello, "An MTL theory approach for the simulation of MIMO power-line communication channels," *IEEE Transactions on Power Delivery*, vol. 26, no. 3, pp. 1710–1717, Jul. 2011.

[52] M. Zimmermann and K. Dostert, "A multipath model for the powerline channel," *IEEE Transactions on Communications*, vol. 50, no. 4, pp. 553–559, Apr. 2002.

[53] A. M. Tonello, "Wideband impulse modulation and receiver algorithms for multiuser power line communications," *EURASIP Journal on Advances in Signal Processing*, pp. 1–14, 2007.

[54] S. Galli, "A simplified model for the indoor power line channel," in *Proceedings of the IEEE International Symposium on Power Line Communications and Its Applications (ISPLC)*, Mar. 2009, pp. 13–19.

[55] A. Pittolo, A. M. Tonello, and F. Versolatto, "Performance of MIMO PLC in measured channels affected by correlated noise," in *Proceedings of the IEEE International Symposium on Power Line Communications and its Applications (ISPLC)*, 2014.

[56] F. Versolatto and A. M. Tonello, "PLC channel characterization up to 300 MHz: Frequency response and line impedance," in *IEEE Globecom*, Dec. 2012, pp. 3525–3530.

[57] J. A. Cortés, "Modulation and multiple access techniques for indoor power-line communications," Available for download from: http://www.plc.uma.es, Ph.D. dissertation, ETSI de Telecomunicación, Universidad de Málaga., 2007.

[58] F. Cañete, J. Cortés, L. Díez, and J. Entrambasaguas, "Modeling and evaluation of the indoor power line transmission medium," *IEEE Communications Magazine*, vol. 41, no. 4, pp. 41–47, 2003.

[59] J. A. Cortés, F. J. Cañete, and L. Díez, "Channel estimation for OFDM-based indoor broadband power line communication systems," *Journal of Communications and Networks*, vol. 25, no. 2, pp. 151–166, Apr. 2023.

[60] J. A. Cortés, *Twenty-five years of PLC channel modelling*, Invited speech at IEEE International Symposium on Power Line Communications and its Applications (ISPLC), Mar. 2023.

[61] F. J. Cañete, J. A. Cortés, L. Díez, J. T. Entrambasaguas, and J. L. Carmona, "Fundamentals of the cyclic short-time variation of indoor power-line channels," in *Proceedings of the International Symposium on Power Line Communications and its Applications (ISPLC)*, 2005, pp. 157–161.

[62] D. Righini, N. A. Letizia, and A. M. Tonello, "Synthetic power line communications channel generation with autoencoders and GANs," in *Proceedings of the IEEE International Conference on Communications, Control, and Computing Technologies for Smart Grids (SmartGridComm)*, 2019.

[63] H. Philipps, "Modelling of power line communication channels," in *Proceedings of the International Symposium on Power Line Communications and its Applications (ISPLC)*, 1999, pp. 14–21.

[64] M. Babic, M. Hagenau, K. Dostert, and J. Bausch, "D4: Theoretical Postulation of PLC Channel Model," Opera, Tech. Rep., 2005.

[65] S. Galli, "A novel approach to the statistical modeling of wireline channels," *IEEE Transactions on Communications*, vol. 59, no. 5, pp. 1332–1345, May 2011.

[66] J. A. Cortés, L. Díez, F. J. Cañete, and J. L. González Moreno, "On the statistical properties of indoor power line channels: Measurements and models," in *Proceedings of the IEEE International Symposium on Power Line Communications and its Applications (ISPLC)*, Mar. 2011, pp. 271–276.

[67] M. Tlich, A. Zeddam, A. Moulin, and F. Gauthier, "Indoor power-line communications channel characterization up to 100 MHz-Part I: One-parameter deterministic model," *IEEE Transactions on Power Delivery*, vol. 23, no. 3, pp. 1392–1401, 2008.

[68] A. Pittolo and A. M. Tonello, "A synthetic statistical MIMO PLC channel model applied to an in-home scenario," *IEEE Transactions on Communications*, vol. 65, no. 6, pp. 2543–2553, Jun. 2017.

[69] I. Povedano, F. Crespo, J. A. Cortés, F. J. Cañete, and L. Díez, "A statistical model for indoor SISO PLC channels," in *Proceedings of the IEEE International Symposium on Power Line Communications and its Applications (ISPLC)*, 2023.

[70] P. Pagani and A. Schwager, "A statistical model of the in-home MIMO PLC channel based on European field measurements," *IEEE Journal on Selected Areas in Communications*, vol. 34, no. 7, pp. 2033–2044, Jul. 2016.

[71] R. Cortina, G. Pioltini, S. Celozzi, and M. D'Amore, "Telecommunication systems on power distribution networks: High frequency performances of carrier channels," *IEEE Transactions on Power Delivery*, vol. 9, no. 2, pp. 654–660, Apr. 1994.

[72] O. G. Hooijen, "On the relation between network-topology and power line signal attenuation," in *Proceedings of the International Symposium on Power Line Communications and its Applications (ISPLC)*, 1998, pp. 45–56.

[73] T. Sartenaer and P. Delogne, "Powerline cables modelling for broadband communications," in *Proceedings of the International Symposium on Power Line Communications and its Applications (ISPLC)*, 2001, pp. 331–337.

[74] F. J. Cañete, L. Díez, and J. T. Entrambasaguas, "Indoor power-line communications: Channel modelling and measurements," in *Proceedings of the International Symposium on Power-Line Communications and its Applications (ISPLC)*, 2000, pp. 117–122.

[75] F. J. Cañete, J. A. Cortés, L. Díez, and J. T. Entrambasaguas, "A channel model proposal for indoor power line communications," *IEEE Communications Magazine*, vol. 49, no. 12, pp. 166–174, Dec. 2011.

[76] A. M. Tonello and F. Versolatto, "Bottom-up statistical PLC channel modeling Part I: Random topology model and efficient transfer function computation," *IEEE Transactions on Power Delivery*, vol. 26, no. 2, pp. 891–898, 2011.

[77] J. A. Cortes, L. Diez, F. J. Canete, and J. Lopez, "Analysis of the periodic impulsive noise asynchronous with the mains in indoor PLC channels," in *Proceedings of the IEEE International Symposium on Power Line Communications and Its Applications (ISPLC)*, 2009, pp. 26–30.

[78] T. Esmailian, F. R. Kschischang, and P. G. Gulak, "In-building power lines as high-speed communication channels: Channel characterization and a test channel ensemble," *International Journal of Communications*, vol. 16, pp. 381–400, Jun. 2003.

[79] I. Kalet, "The multitone channel," *IEEE Transactions on Communications*, vol. 37, no. 2, pp. 119–124, 1989.

[80] L. T. Berger, A. Schwager, P. Pagani, and D. M. Schneider, "MIMO power line communications," *IEEE Communications Surveys & Tutorials*, vol. 17, no. 1, pp. 106–124, 2015.

[81] D. Righini and A. M. Tonello, "Characterization and exploitation of quasi determinism in multi-conductor power line communication noise," *IEEE Open Journal of the Communications Society*, vol. 2, pp. 809–1825, Jul. 2021.

[82] C. R. Paul, *Analysis of Multiconductor Transmission Lines* (Wiley Series in Microwave and Optical Engineering). Wiley, 1994.

[83] *Proteus - Circuit Simulation Software with SPICE*, `https://rb.gy/pdjayc`.

[84] T. Dhaene and D. De Zutter, "Selection of lumped element models for coupled lossy transmission lines," *IEEE Transactions on Computer-Aided Design*, vol. 11, no. 7, pp. 805–815, Jul. 1992.